Pushing the limits of resolving power and analysis time in on-line comprehensive hydrophilic interaction x reversed phase liquid chromatography for the analysis of complex peptide samples

Soraya Chapel, Florent Rouvière, Sabine Heinisch

Pushing the limits of resolving power and analysis time in on-line comprehensive hydrophilic interaction x reversed phase liquid chromatography for the analysis of complex peptide samples

Soraya CHAPEL, Florent Rouvière,-Sabine Heinisch*

Université de Lyon, Institut des Sciences Analytiques, UMR 5280, CNRS, ENS Lyon, 5 rue de la Doua, 69100, Villeurbanne

* Corresponding author: Tel: +33 437 423 551;
E-mail address: sabine.heinisch@univ-lyon1.fr (Sabine Heinisch)

ABSTRACT

In the present work, we have investigated the combination of hydrophilic interaction liquid chromatography (HILIC) and reversed phase liquid chromatography (RPLC) for the separation of peptides in on-line HILIC x RPLC. This combination usually leads to significant solvent strength mismatch, since a weak solvent in HILIC becomes a strong solvent in RPLC. This may result in band broadening, peak distortion, and breakthrough phenomena. Our focus was directed towards the reduction of band broadening and peak distortion. The conditions of the emergence of breakthrough could be investigated with high resolution mass spectrometry (HRMS) detection. The importance of both the injection volume and the difference in composition between injection and elution solvents was highlighted. Reported strategies to avoid bad peak shapes mostly rely either on flow splitting to limit the injection volume, or on on-line dilution. Here, we propose an alternative approach which consists in injecting large volumes in the second dimension. In this case, no flow-splitting nor dilution prior to the second dimension is required. Our results show that above a certain critical injected volume, depending on both the compound and the elution conditions, narrow and symmetrical peaks can be obtained, despite the persistence of breakthrough. As a result, the injected volume in the second dimension must be larger than the largest critical volume. This counter-intuitive approach was applied for the on-line HILIC x RPLC-UV-HRMS analysis of a complex tryptic digest sample. A peak capacity close to 1500 could be achieved in 30 minutes, which is two-fold higher than in RPLC x RPLC within the same analysis time.

Keywords

Two-dimensional liquid chromatography; HILIC x RPLC-HRMS; Peptides; Breakthrough; solvent strength mismatch

1. Introduction

Protein enzymatic digests can contain hundreds of compounds with a wide range of molecular weights, polarity, and hydrophobicity, which makes their complete separation hardly achievable using conventional one dimensional liquid chromatography (1D-LC). The performance of LC coupled to mass spectrometry (LC-MS) is most often hindered by matrix effects, arising from co-eluting compounds interfering with ionization efficiency. Despite the unarguable selectivity of MS detection, a high separation power is required in LC to simplify the matrix entering MS. In the quest for higher peak capacities, on-line comprehensive two-dimensional liquid chromatography (LC x LC) has emerged as an attractive technique to overcome the limitations of 1D-LC. The peak capacity in LC x LC is theoretically expected to be the product of the peak capacities in both dimensions [1]. Actually, the effective peak capacity in on-line LC x LC can be much lower due to the combination of three effects: (i) first dimension (^{1}D) under-sampling, (ii) incomplete coverage of the retention space, and (iii) non-ideal fraction transfer between both dimensions [1–4]. Combining two similar retention mechanisms such as reversed phase liquid chromatography (RPLC x RPLC), has been shown to be attractive for the separation of peptides [5–9], provided that the mobile phase conditions in both dimensions were well selected (i.e. organic modifiers, additives, pHs, flow rates and/or temperatures). One of the benefit of such approach is that fairly good peak shapes can be obtained in the second dimension (^{2}D) thanks to the compatibility of the ^{1}D-mobile phase with the ^{2}D-separation. However, because the two dimensions are partially correlated, the peaks usually distribute themselves around the diagonal of the 2D-separation space, resulting in a retention space coverage rarely exceeding 60% and hence decreasing the effective peak capacity. The highest reported peak capacity in RPLC x RPLC was found to be close to 5000 in 180 min [6]. That is 3-fold higher than the highest value ever attained in 1D-RPLC (about 1600 in 40 h) [10]. Maximizing the retention space coverage can be achieved by selecting two different chromatographic modes, able to change the selectivity for the compounds of interest. The combination of hydrophilic interaction liquid chromatography (HILIC) and RPLC was proved to be very attractive for the separation of peptides with respect to orthogonality [11]. Their respective mobile phases are fully miscible. However, the weaker solvent in HILIC being the stronger solvent in RPLC and vice-versa, their coupling usually leads to severe injection effects in ^{2}D, including band broadening, peak distortion and breakthrough phenomena [7,9,12–14]. This latter is the occurrence of two distinct peaks for the

same compound: one, not retained, and one, retained, with most often severe peak fronting. This so-called “solvent strength mismatch” is one of the most cited challenges when combining HILIC and RPLC. Solvent strength mismatch has a strong impact on the ^{2}D chromatographic performance, resulting in a dramatic loss of peak capacity and peak intensity. For that reason, the coupling of HILIC and RPLC is often performed in the off-line mode [15–17], which allows to evaporate the ^{1}D collected fractions for further injection in ^{2}D in a weaker solvent. Both dimensions being connected in the on-line mode, the ^{2}D injection solvent composition cannot be easily controlled, resulting in strong injection solvents in ^{2}D. The combination of HILIC and RPLC for on-line LC x LC has been widely used. Among the large variety of applications, surfactants [18–20], saponins [21] phenolics [22–26], lipids [27] and ginsenosides [13,28,29] can be cited. Most of them were performed with HILIC as first dimension separation. As regards peptide analysis, both on-line RPLC x HILIC [7] and HILIC x RPLC [5,9] were used. If the order in which the two chromatographic modes are connected should not impact the degree of orthogonality, it can play a significant role on 2D-LC performance. The potential advantage in RPLC x HILIC for peptide analysis is that a large volume can be injected in ^{1}D-RPLC without affecting column efficiency, considering the aqueous medium of the digest. In similar conditions, ^{1}D-HILIC should lead to severe injection effects, thereby decreasing both peak capacity and peak intensity. The high content of acetonitrile (ACN) in ^{2}D mobile phase is also a clear advantage in RPLC x HILIC, since it allows faster ^{2}D separations and better MS signal intensity. However, a major drawback of ^{2}D-HILIC is the need for long equilibration times [30], reducing the available gradient time in ^{2}D and thus the peak capacity. Furthermore, due to their quadratic retention behavior in HILIC [7], peptides may be not eluted during the gradient time if this latter is short, as required in ^{2}D.

In view of the above, we focused on on-line HILIC x RPLC for the separation of tryptic digests. Several strategies were proposed to limit the negative impact of the ^{1}D-HILIC mobile phase on the ^{2}D-RPLC separation. They mostly rely either on reducing the ^{2}D injection volume [23,24,31–33], or on using active modulation techniques (on-line dilution with or without trapping column) to decrease the eluent strength of the ^{1}D mobile phase before entering the ^{2}D column [13,14,20,22,26–29,34].

The objective of this work was to propose an easy and alternative way to overcome the deleterious impact of solvent strength mismatch in on-line HILIC x RPLC. In each dimension, the impact of injection conditions on peak shapes was deeply investigated. Special emphasis was put on reducing the negative impact of the ^{1}D-mobile phase on the ^{2}D-separation. An alternative strategy relying on the injection of large volumes of fractions in ^{2}D-RPLC is proposed. The applicability and potential of such approach is illustrated with the separation of a protein tryptic digest and both ultraviolet (UV) and high-resolution mass spectrometry (HRMS) detections.

2. Experimental section

2.1. Chemicals and reagents

Acetonitrile (LC-MS grade) was obtained from Sigma-Aldrich (Steinheim, Germany). Water was purified and deionized by an Elga Purelab Classic UV purification system (Veolia water STI, Le Plessis Robinson, France). Formic acid (LC/MS grade), ammonium acetate and ammonium bicarbonate (both analytical reagent grade) were obtained from Fischer scientific (Illkirch, France). DL-1,4-dithiothreitol (DTT, 99%) and iodoacetamide (98%) were obtained from Acros Organics (Geel, Belgium). Trypsin, human serum albumin (HSA), bovine serum albumine (BSA), β-casein, myoglobin, lysozyme, and cytochrom C were all obtained from Sigma-Aldrich (Steinheim, Germany). Influenza hemaglutinin (HA), FLAG® peptide, leucine encephalin, bombesin, [arg8]-Vasopressin, [ile]-Angiotensin, bradykinin fragment 1-5, substance P, and bradykinin were obtained from Merck (Molsheim, France). WDDHH was custom synthesized (Genecust, Luxembourg). The physical properties of the ten peptide standards are listed in Table 1.

2.2. Sample preparation

A peptide sample was obtained from the tryptic digestion of six proteins (HSA, BSA, β-casein, myoglobin, lysozyme and cytochrome C) according to a protocol described elsewhere [6]. The concentration in each protein was 4000 mg/L and the protocol led to a tryptic digest containing 196 peptides with an average concentration per peptide of 120 mg/L. Aliquots of the tryptic digest were stored at -20 °C in polypropylene tubes. The samples were thawed and filtered on a 0.22 µm low protein binding PVDF (polyvinylidene fluoride) membrane before injection. In order to study the impact of the sample solvent on peak shapes in HILIC, the tryptic digest was diluted with acetonitrile (ACN) resulting in samples with different sample solvent compositions: 0:100 (no dilution), 50:50 (2-fold dilution), 75:25 (4-fold dilution), or 90:10 ACN/water (10-fold dilution) (v/v). The composition of the sample solvent for the developed 2D-method was 50:50 ACN/water (v/v), resulting in an average concentration per peptides of 60 mg/L.

For the study of injection effects in HILIC, the concentrations of the peptide standards were either 42 mg/L with different solvent compositions including 0:100, 25:75, 50:50, and 75:25 ACN/water (v/v), or 21, 10.5, and 4.2 mg/L with 50:50, 75:25, and 90:10 ACN/water (v/v), respectively.

For the screening of HILIC columns, the sample solvent for the tryptic digest was 50:50 ACN/water (v/v). Peak widths, peak heights and peak asymmetries were determined from peptide standards at a concentration of 42 mg/L in 75:25 ACN/H_2O (v/v).
For the study of overloading effects in RPLC, peptide #4 was diluted at a concentration of 16, 80, or 160 mg/L in 30:70 water/ACN (v/v). The study of injection effects in RPLC was performed with both peptide #4 and peptide #6 (see Table 1) diluted at a concentration of 50 mg/L in 90:10, 70:30, 50:50, 30:70, and 10:90 water/ACN (v/v). For the linearity study in RPLC, peptide #4 was diluted at different concentration ranging from 5 to 500 mg/L in 30:70 water/ACN (v/v). The peptide standard solutions were all stored at -20 °C and uses within a week after thawing.

2.3. Columns

The characteristics of the ten columns evaluated in HILIC are summarized in Table 2. Three columns were used in RPLC: Kinetex C18 (30 mm x 2.1 mm, 1.3 µm) from Phenomenex (Torrence, CA, USA), Acquity CSH C18 (30 mm x 2.1 mm, 1.7 µm) from Waters (Milford, MA, USA), and Ascentis express C18 (50 mm x 2.1 mm, 2.7 µm) from Sigma-Aldrich (Saint-Louis, MO, USA).

2.4. Instrumentation

For studies in 1D-LC, experiments were carried out with an Acquity UPLC I-Class liquid chromatography system (Waters, Milford, MA, USA). The instrument includes an high-pressure binary solvent delivery pump, a sample manager with a flow through needle injector of 15 µL equipped with an additional extension loop of 100 µL, a column manager equipped with a column oven with a maximum temperature of 90 °C, and a photodiode-array detector (PDA) equipped with a 0.5 µL flow-cell withstanding pressure up to 70 bar. The dwell volume and the extra-column volume for this entire system were measured using a zero dead volume union connector in place of the column, and were respectively 110 µL and 12 µL (without extension loop). The 1D-LC system was hyphenated to a Waters Acquity QDa mass spectrometer, used in scan mode and in single ion recording (SIR) mode. A T-connection was placed right after the column to decrease the flow rate entering the mass spectrometer by half (split ratio 1:1) when the flow rate was 1.5 mL/min. Data acquisition and instrument control were performed using Waters MassLynx software.
On-line LC x LC experiments were carried-out using an Infinity 1290 2D-LC system (Agilent technologies, Waldbronn, Germany). The instrument includes two high-pressure binary solvent delivery pumps, an autosampler with a flow-through needle of 20 µL, two thermostated column

compartments with a maximum temperature of 100 °C equipped with low-dispersion preheaters, and two diode-array detectors (DAD) equipped with 0.6 µL flow-cells. The interface connecting the two dimensions consisted in a 2-position /4-port duo valve, equipped with two identical 20 µL or 40 µL loops, depending on the transferred volume. In order to minimize dispersion, the valve was configured in back-flush injection mode. A pressure release kit placed between the ^{1}D outlet and the interface was used to minimize the pressure downstream induced by the switch of the 2D-LC valve in order to protect the ^{1}DAD flow-cell and to avoid artefacts in the ^{1}DAD signal. The measured dwell volumes and extra-column volumes of this 2D-LC system were respectively 140 µL and 22 µL in ^{1}D, and 45 µL and 8.5 µL in ^{2}D (loop volumes at the interface excluded). The 2D-LC system was hyphenated to an Agilent G6545B Q-TOF mass spectrometer, equipped with a JetStream electrospray ionization (ESI) source. Data acquisition and instrument control were performed using Agilent OpenLab software for 2D-LC and MassHunter software for MS. MS data processing was performed using Agilent MassHunter qualitative analysis software for MS data. LC x LC data were processed using an in-house script developed on Matlab.

2.5. Chromatographic and detection conditions

2.5.1. 1D-HILIC conditions

The optimization of injection conditions in HILIC was performed on the Acquity BEH Amide column (50 mm x 2.1 mm, 1.7 µm). The mobile phase was composed of ACN as solvent A and water with 10 mM ammonium acetate (pH = 6.8) as solvent B. The aqueous eluent prepared with salts was filtered on 0.22 µm nylon filter before use. The gradient elution was as follows: from 2% to 60% B in 29 t_0 (with t_0, the column dead time calculated according to Eq.3), from 60% to 2% B in 1 t_0, and 2% B during 10 t_0. The different injection volumes were about 1%, 2%, 5%, and 10% V_0 (with V_0, the column dead volume calculated according to Eq.4).

The comparison of columns in HILIC was performed with the ten columns listed in Table 2 and the following gradient elution: from 2% to 42% B in 20 t_0, 42% during 5 t_0, from 42% to 2% in 1 t_0, and 2% during 10 t_0. The flow rates for column #2 was set at 0.6 mL/min, and other flow rates were calculated according to Eq.1.The column temperature was set to 30 °C and the injected volume represented either 0.5% V_0 (for the peptide standards) or 5% V_0 (for the tryptic digest).

UV absorbance data were collected at 210 nm with an acquisition rate of 20 Hz. MS data were acquired from m/z 100 to m/z 1200 in negative electrospray ionization (ESI^-) mode at an acquisition rate of 10 Hz. The cone voltage was set to 15 V and the capillary voltage to 0.8 kV. The source and the probe temperature were set at 120 °C and 600 °C, respectively.

2.5.2. 1D-RPLC conditions

Kinetex C18 (30 mm x 2.1 mm, 1.3 µm) and Acquity CSH C18 (30 mm x 2.1 mm, 1.3 µm) columns were compared. The mobile phase was composed of water with 0.1% formic acid as solvent A, and ACN with 0.1% formic acid as solvent B (pH = 2.7). The gradient elution was as follows: from 1% to 45% B in either 44 or 5.5 t_0, from 45% to 1% B in 1 t_0, and 1% B during 5 t_0. The flow rate was 1.5 mL/min, and the column temperature was either set to 90 °C for the Kinetex column, or 80 °C for the Acquity CSH column. The different injection volumes were about 1%, 2%, or 6% V_0.

The optimization of injection conditions in RPLC was performed with the same conditions, but with a gradient ranging from 1% to 45% B in 11.3 t_0. Different volumes ranging from 0.5% to 100% V_0 were injected. UV absorbance data were collected at 210 nm with an acquisition rate of 40 Hz. The effluent from the column was split 1:1 prior to the mass spectrometer using a simple T-connection. MS data acquisition conditions were the same as for 1D-HILIC, but in positive electrospray ionization (ESI^+) mode. The mass of the standards of peptide #4 and #6 were monitored in selected ion recording (SIR) mode with m/z 556.6 for peptide #4 and m/z 542.6 for peptide #6.

2.5.3. On-line LC x LC conditions

In HILIC x RPLC, ^{1}D was performed using an Acquity BEH HILIC column (50 mm x 2.1 mm, 1.7 µm). The injected volume was 6 µL (5% V_0). The mobile phase was the same as for ^{1}D-HILIC and the gradient was: 0 min (2% B), 30 min (52% B), 32.4 min (2% B), and 50 min (2% B). The flow rate was 0.05 mL/min and the column temperature was 30 °C. ^{2}D was performed on an Acquity CSH C18 column (30 mm x 2.1 mm, 1.7 µm). The mobile phase was the same as for 1D-RPLC, and the gradient was: 0 min (1% B), 0.26 min (45% B), 0.29 min (1% B), and 0.39 min (1% B). The flow rate was 2 mL/min and the column temperature was 80 °C. The sampling time was 0.39 min, leading to an injection volume of 19.5 µL (27 % V_0) in ^{2}D. In two other comparative 2D-experiments, the effluent from ^{1}D was split 1:1 or 1:3 with a T-piece, leading to injection volumes of 9.8 µL (14 % V_0), or 4.9 µL (7% V_0), respectively.

In RPLC x RPLC, ^{1}D was performed using an Ascentis express C18 column (50 mm x 2.1 mm, 2.7 µm). The injected volume was 10 µL (12% V_0). The mobile phase was the same as for 1D-HILIC and the gradient was: 0 min (1% B), 30 min (34% B), 32.2 min (1% B), and 45 min (1% B). The flow rate was 0.04 mL/min, and the column temperature was 30 °C. ^{2}D conditions were similar as in HILIC x RPLC, with gradient: 0 min (1% B), 0.13 min (45% B), 0.16 min (1% B), and 0.27 min (1% B). The flow rate was 1.5 mL/min and the column temperature was 90 °C. The sampling time was 0.27 min and a split

ratio of 1:2 led to an injection volume of 3.6 µL (5 % V_0) in ^{2}D. LC x LC parameters were optimized with an in-house 2D prediction tool based on a Pareto-optimality approach described by Sarrut et al [6].

For both experiments, the effluent from the ^{2}D-column was split between MS and UV (1:2) using a T-connection. UV absorbance data were collected at 210 nm, with acquisition rates of 20 Hz and 40 Hz in ^{1}D and ^{2}D, respectively. QTOF-HRMS data were acquired in positive ion mode from m/z 100 to m/z 3200 at an acquisition rate of 20 spectra/s. The drying gas temperature and flow rate was 300 °C and 11 L/min, respectively. The nebulizer gas pressure was 40 psi. The sheath gas temperature and flow rate was 350 °C and 11 L/min, respectively. The capillary, the nozzle, the fragmentor, the skimmer and the Oct 1 RV voltages were 3500, 300, 150, 20 and 750 V, respectively. The conditions of the 2D-separations are recapitulated in Table 3.

2.6. Calculations

The flow rate in HILIC for column #2 (see Table 2) was set at 0.6 mL/min. Other flow rates were selected according to the following transfer rule:

$$F_n = F_2 \left(\frac{d_{i,n}}{d_{i,2}}\right)^2 \times \left(\frac{d_{p,2}}{d_{p,n}}\right) \quad \text{(Eq.1)}$$

F_2, $d_{i,2}$, *and* $d_{p,2}$ are the flow rate, the inner diameter, and the particle diameter of column #2, respectively. F_n, $d_{i,n}$, and $d_{p,n}$ are those of a given column #n.

The composition at elution, C_e, was calculated according to:

$$C_e = C_i + \frac{C_f - C_i}{t_G} \times (t_r - t_0 - t_D) \quad \text{(Eq.2)}$$

C_i and C_f are the initial and final composition of strong solvent (%B). t_G, t_r, t_0, and t_d are the gradient time, the retention time of the compound, the column dead time, and the instrument dwell time, respectively.

The column dead time (t_0) was calculated according to:

$$t_0 = \frac{V_0}{F} \quad \text{(Eq.3)}$$

V_0 is the column dead volume, estimated by:

$$V_0 = \frac{\pi L d_i^2 \varepsilon}{4} \quad \text{(Eq.4)}$$

L, d_i, and ε are respectively the column length, the column inner diameter, and the total column porosity (estimated as 0.5 for superficially porous, and 0.7 for totally porous particles).

Experimental peak capacities for 1D-LC separations and for each dimension in LC x LC were calculated according to:

$$n_{exp} = 1 + \frac{t_n - t_1}{w_{4\sigma}} \quad \text{(Eq.5)}$$

t_n and t_1 are the retention times of the last and first eluted compound, respectively, and $w_{4\sigma}$ is the average peak width at 4σ (i.e. 13.4% of peak height).

Theoretical peak capacities in HILIC were predicted according to Linear Strength solvent (LSS) theory [35] with the following equation:

$$n_{1D,th} = 1 + \frac{2.3S \times \Delta C}{2.3b + 1} \times \frac{\sqrt{N}}{4} \quad \text{(Eq. 6)}$$

N is the column plate number, estimated by:

$$N = \frac{L}{3d_p} \quad \text{(Eq.7)}$$

S is the average value of the slope of the relationship between the logarithm of the retention factor k and the solvent composition C (%) ($\log(k) = \log(k_0) - S \times C$). An average S value of 0.06 was used for calculations in HILIC based on previous studies [8]. k_0, ΔC_e, b, and L are the retention factor in the weaker solvent, the range of composition at elution, the gradient steepness ($b = S\Delta C t_0 / t_G$, with ΔC, the gradient composition range), and the column length, respectively.

Effective experimental peak capacities in on-line LC x LC were calculated according to:

$$n_{2D,effective} = \alpha \times \gamma \times {}^{1}n_{exp} \times {}^{2}n_{exp} \quad \text{(Eq.8)}$$

303

304 ${}^{1}n_{exp}$ and ${}^{2}n_{exp}$ are the experimental peak capacities (Eq. 5) in ^{1}D and ^{2}D, respectively. α is a correction
305 factor, taking into account under-sampling in ^{1}D and calculated according to [36]:

306

307 $$\alpha = \frac{1}{\sqrt{1 + 0.21\left({}^{6}/_{\tau}\right)}} \quad \text{(Eq.9)}$$

308

309 τ is the sampling rate (i.e. number of fractions per 6σ ^{1}D-peak), and γ is a correction factor which
310 takes into account the retention space coverage of the 2D separation. The evaluation of γ was made
311 using a method described elsewhere [8].

312

313 **3. Results and discussion**

314

315 3.1. Preliminary search for optimal conditions in each dimension

316

317 A separation in 2D-LC is the combination of two 1D-LC experiments. As part of method
318 development, each separation was first individually optimized. The nature of the stationary phase,
319 the mobile phase conditions and the injection conditions (i.e. injection solvent and injection volume)
320 were deeply investigated in order to find the best trade-off between high peak capacity, high peak
321 intensity, and short analysis time. In our context of complex sample analysis, special emphasis was
322 put on improving the kinetic performance of the separation (i.e. peak shape, peak width and peak
323 asymmetry) in both dimensions, in order to maximize the overall separation power. This first part
324 details the choices that were made in each dimension, with respect to the chromatographic
325 conditions, before developing on-line HILIC x RPLC.

326

327 3.1.1.Optimization of injection conditions in HILIC

328

329 HILIC mobile phases contain a high percentage of ACN (generally 98 to 50%) while a low percentage
330 of water (2 to 50%). Numerous papers showed the negative impact of an injection solvent too rich in
331 water on HILIC separation [37–39]. It is therefore recommended to minimize as much as possible the
332 amount of water in the injection solvent to maintain proper peak shapes in HILIC. For example,
333 significant band broadening and peak distortion were reported for peptides in the range 1000 to
334 6000 Da when the water content exceeded 10% (v/v) with injection volumes as low as 1.5% V_0 [39].
335 The tryptic digest being prepared in water, we investigated the impact of both injection solvent and
336 injection volume on peak shape. The study was carried out in gradient elution with an Acquity BEH

amide column. Injection effects were evaluated from ten representative peptides (see Table 1), individually injected. The injection solvent composition was in the range 0:100 to 75:25 ACN/H_2O (v/v) while the injection volumes were in the range 1% to 10% V_0. Fig. 1 illustrates the impact of the injection solvent on the peak shape of peptide #4 (Fig. 1a) and peptide #8 (Fig. 1b), eluted at two different compositions, 13% and 25% water, respectively. As expected, the peak shape got worse when the percentage of water in the injection solvent increased. For peptide #4, symmetrical peaks were obtained up to 50% water. Peak broadening and peak splitting were observed beyond in spite of an injected volume as low as 1% V_0. Appropriate peak shapes were obtained for a more retained peptide (i.e. #8) with injected volume up to 10% V_0 and 50% water in the injection solvent (Fig. 1b). This is in good agreement with a previous study, showing that early eluted compounds are more affected than later eluted ones [39]. It is therefore of prime importance to decrease the water content of the injection solvent. The tryptic digestion being prepared in water, reducing the water content leads to sample dilution. Fig. 2 shows the chromatograms of peptide #4 (Fig. 2a) and peptide #8 (Fig. 2b), obtained with no dilution, 2-fold, 4-fold and 10-fold dilution with ACN (i.e. 0%, 50%, 75%, and 90% ACN) while maintaining the same amount of peptide by varying the injection volume (1%, 2%, 4% and 10% V_0). As can be observed, the peak shape of the least retained peptide (Fig. 2a) gets better and better by increasing dilution. A symmetrical peak could be obtained up to a 10-fold dilution despite the corresponding large injection volume (10% V_0). However, for the most retained peptide (Fig. 2b), the dilution appears to be useless since the peak shape is kept identical without and with any dilution. For the ten studied peptides, the peak areas did not vary with dilution, suggesting that they were fully soluble up to 90% ACN (10-fold dilution). However, it was not the case for the tryptic digest (Fig.3). The peak intensities were drastically reduced with 90% ACN which can be ascribed to a decrease in the peptide solubility and hence to partial sample precipitation as also shown for hydrophilic compounds in ACN-rich solvents [39]. It should be also noted in Fig.3 that peak intensities are lower with no dilution (100% water) than with 2-fold dilution (50% water), which can be explained by the occurrence of a breakthrough phenomenon. Alternative solvents such as methanol, ethanol, or isopropanol were also used to dilute the sample as suggested for peak shape improvement [39]. However replacing acetonitrile by these solvents also led to sample precipitation beyond 50% organic solvent. The use of a sandwich injection as reported for the HILIC separation of very large proteins [14] was also investigated. Various ratio of ACN/sample and ACN/sample/ACN were evaluated. However no improvement in peak shape could be observed. In light of the above results, a 2-fold sample dilution (50% ACN) with an injection volume of 6 µL (5% V_0) were selected for the rest of the study. Under such conditions, satisfactory peak shapes could be obtained for most eluted peptides.

Considering the obtained separation (Fig. 3), the elution range for peptides was found to be 13% to 52% water. However the initial composition was set at 2 % water to promote the dilution of the water-rich injection plug (50%) with the ACN-rich gradient starting conditions (98%). The peak shapes could be significantly improved for early eluted compounds compared to a gradient starting from 13% water (see Supplementary Information S1).

3.1.2.Selection of the stationary phase in HILIC

The mobile phase was composed of ACN as solvent A and ammonium acetate (10 mM dissolved in water) as solvent B, according to previous studies on the separation of peptides in HILIC [7,8]. Ten different stationary phases were evaluated. The related phase chemistries include bare silica, hybrid silica, NH_2-bonded silica, charged silica, and zwitterionic-bonded silica. Their characteristics and specific operating conditions are listed in Table 2. A generic method involving a linear gradient elution from 2% B to 42% B in 20 t_0 (followed by an isocratic hold during 5 t_0 to ensure complete elution) was used. Column performance was evaluated by injecting a tryptic digest composed of six proteins diluted in 50:50 ACN/water (5% V_0 injected) and ten individual peptide standards (Table 1) diluted in 75:25 ACN/water (0.5% V_0 injected). Such injection conditions for the peptides aimed at preventing any injection effect according to the above discussion. The obtained separations for the tryptic digest are shown in Fig. 4. The separations for the peptides are given in Supplementary Information S2. Significant differences can be observed in Fig. 4 between columns with different chemistry (e.g. #1, #3, #5, and #9), but also between bare silica columns coming from different providers (e.g. #2 and #4), or even from the same provider (e.g. #1 and #4). The most striking difference between columns concerns column #4 (bare silica) as opposed to other bare silica columns (#1, #2, #6, #8, or #10). It is also worth noting the marked difference between the zwitterionic columns #5 (bad separation) and #7 (fairly good separation). In contrast, the separations obtained on superficially porous bare silica phases (#6, #8, and #10) are quite similar. Concerning the peptide samples, some significant differences were observed for both the peak shapes and the retention orders between columns (Supplementary Information S2). Four quality descriptors including peak capacity, peak asymmetry, number of observed peaks, and elution window (% B) were used to assess the column performances. The first two were measured from the separations of the peptide samples, while the last two, from the separations of the tryptic digest (Fig.4). The resulting values are summarized in Table 2. The peak capacity which is a key quality descriptor for complex sample analysis, was measured by considering the average 4σ peak width of three well

distributed peptides (i.e. #1, #4, and #7) and the elution window (Eq.2). For a fair comparison, the peak capacity is here given as the ratio of the experimental (Eq.5) to the theoretical value (Eq.6). The highest values (> 0.6) were found for two bare silica columns (#1 and #2), while the lowest ones (< 0.35) for the two zwitterionic columns (#5 and #7). No particular correlation between the phase chemistry and the elution window or the peak asymmetry could be found. The final selection was made by the calculation of a desirability function [40], corresponding to the geometric mean of the four quality descriptors transformed into four functions varying from 0 to 1 (see Supplementary Information S4). According to the resulting values (Table 2), columns #1 and #2 are the most suitable ones for peptides, while columns #5, and #6 are the least advantageous ones. The best columns (#1 and #2) are both made of bare silica. With a view to keeping the analysis time as short as possible, the Acquity BEH HILIC column (#2) was selected for ^{1}D-HILIC.

3.1.3.Selection of the stationary phase in RPLC

The choice of water, ACN, and formic acid (0.1%) in RPLC was supported by our previous studies on peptides [7,8]. Due to the need for very fast separations in ^{2}D in on-line LC x LC [2], HT-UHPLC (high temperature ultra-high performance liquid chromatography) conditions were selected, with both temperature and flow rate set at the maximum authorized values. For the same reasons, ACN was preferred to methanol due to its lower viscosity. Formic acid was selected for two main reasons: (i) acidic pH is highly recommended at high temperature to prevent column degradation, and (ii) this additive is much better than TFA (trifluoroacetic acid) for MS detection, although less attractive from a separation point of view. In fact due to the resulting low ionic strength of the mobile phase, formic acid (0.1%) may lead to overloading effects with charged compounds [41,42], leading to peak distortion and hence to poor LC x RPLC performance[7]. In order to achieve ultra-fast separations in ^{2}D, a short column packed with very small particles was first considered. The Kinetex C18 column (30 mm x 2.1 mm, 1.3 µm) was very attractive considering its low particle size (1.3 µm) and its successful use for the separation of peptides in on-line RPLC x RPLC [6]. However, in the present study, we found significant overloading effects under certain conditions. Those are highlighted in Fig. 5, showing overlaid peaks of peptide #4, obtained with different injection volumes (0.5 to 3 µL corresponding to 1% to 6% V_0), and two different peptide concentrations: 16 mg/L (Fig.5a) and 80 mg/L (Fig.5b). By increasing the peptide concentration and/or the injected volume while keeping the same gradient time (5.5 t_0), the peak distortion increases with the occurrence of a triangular peak shape. The peak distortion further increases with the gradient time (44 t_0) in Fig. 6a, which is in good agreement with previous results [7]. In the present study, the impact of the injection volume in

addition to the peptide concentration is also clearly highlighted in Fig. 6a. by a gradual shift of the peak apex towards lower retention times. Such overloading effects severely reduce the peak capacity in ^{2}D-RPLC. Furthermore, the retention shift which depends on the solute concentration and hence on the peak fraction in ^{1}D, makes 2D-data very difficult to process [7]. We therefore evaluated an Acquity CSH C18 column (30 x 2.1 mm, 1.7µm). This stationary phase contains positive charges on the silica surface which are designed to reduce overloading effects of basic compounds in acidic media. The resulting overlaid peaks are shown in Fig. 6b and can be compared to those in Fig.6a, obtained with the Kinetex C18 column in the same conditions. As can be observed, the peak shapes are markedly improved with the Acquity CSH C18 column. When increasing concentrations up to 160 mg/L and injection volumes up to 18% V_0, the peak was still kept symmetrical (see Supplementary Information S5), making Acquity CSH C18 much more attractive for ^{2}D-RPLC than Kinetex C18 despite larger particles (1.7 µm vs 1.3 µm). The fact that the peak area did not increase between 2% V_0 and 6% V_0 results from a breakthrough phenomenon which is extensively discussed in the next section. .

3.1.4. Optimization of injection conditions in RPLC

As underlined in Section 3.1.1, the nature of the injection solvent, and the injected volume are two critical parameters in LC, since they may strongly affect the peak shape and thus the chromatographic performance. As a rule, it is usually recommended to match the injection solvent with the initial mobile phase in gradient elution in order to promote on-column focusing. However, unlike in ^{1}D, the injection solvent cannot be controlled in ^{2}D since both dimensions are connected. For peptides, whereas some combinations such as RPLC x RPLC [6,43] or SCX x RPLC [9] are fairly compatible, others may suffer from solvent strength mismatch between both dimensions. In that way, the injection in ^{2}D-RPLC of an ACN-rich solvent coming from ^{1}D-HILIC can lead to band broadening, peak distortion, and sometimes breakthrough phenomena. That makes the combination of HILIC and RPLC very challenging. Usual strategies to limit injection effects in on-line HILIC x RPLC rely either on the reduction of the injection volumes or on the use of active modulation techniques (i.e. on-line dilution with or without trapping columns). Advantages and limits of these strategies will be discussed in detail in a future study. In the present work, we conducted a deep investigation on the impact of both the injection solvent and the injection volume on the peak shape of peptides in RPLC. The focus was directed towards finding the easiest and the most efficient way to reduce band broadening and peak distortion in RPLC, when injecting very strong solvents such as those coming from ^{1}D-HILIC. Fig. 7 shows the variation of the peak shape of peptide #4 in RPLC with different

injection volumes (1.5% to 6.2% V_0) and an injection solvent with a moderate strength in RPLC (50:50 water/ACN (v/v)), considering the range of ACN composition (from 98% to 48% ACN) for the separation of peptides in HILIC. As a result, the chromatograms in Fig.7 illustrate the most favourable injection conditions with respect to the peak shape. When increasing the injected volume from 1 µL (1.5% V_0, Fig. 7a) to 4.5 µL (6.2% V_0, Fig. 7e), the peak evolves from a symmetrical shape to a severe distortion, with furthermore the occurrence of a breakthrough phenomenon, which results in the presence of an intense non-retained peak (shown in Figs.7e and 7f by an asterisk). Up to 4.8 V_0 injected (Figs.7a to 7e), the peaks can be divided into three groups: (i) the first one (Fig. 7a) without any injection effects (injected volume < 1.5% V_0), (ii) the second one (Figs. 7b to 7d) with more or less distortion (peak splitting and/or distortion) but without breakthrough, and (iii) the third one (Fig. 7e) with the apparition of three distinct peaks (one unretained peak of breakthrough in the dead volume, one retained peak eluted at its expected retention time, and a third broad peak between the two). Consequently, increasing injection volumes in RPLC should severely reduce the chromatographic performance in online HILIC x RPLC. The most usual strategy in on-line HILIC x RPLC consists in reducing the injected volume, yet increasing sample dilution in ^{2}D. Our study on a broad range of injection volumes led to surprising observations. When increasing the injection volume above a certain critical value, we found an unexpected fourth group of peaks as shown in Fig. 7f, where a single retained peak could be obtained despite the persistence of breakthrough. In addition, it is interesting to notice its quite symmetrical shape. The comparison of Fig. 7e and Fig. 7f clearly shows that the additional peak, located between the dead time and the retained peak, has entirely disappeared between 4.8% and 6.2% V_0 injected. We called this specific phenomenon “total breakthrough”, in contrast to the earlier stage of breakthrough exhibiting strong peak distortion. Those symmetrical retained peaks were observed with injection volumes up to 50% V_0. Above this volume, the retained peak becomes less symmetrical with increased fronting by further increasing the injected volume. The absence of any peak between the unretained (breakthrough) and the retained peaks was ensured by MS detection. This thorough study on injection effects in RPLC was conducted with several injection solvent compositions ranging from 0% to 90% ACN, and over a broad range of injection volumes ranging from 0.5% V_0 to 100% V_0. The importance of the injection solvent composition, the injection volume, and the difference in composition between injection and elution solvents is highlighted in Fig. 8. This latter shows the variation of the area of the retained peak (peptide #4 eluted with a composition of 16% ACN) with the injection volume (expressed as the ratio of the injected volume to the dead volume) for different injection solvents. The resulting curves clearly underline the different stages related to the evolution of the peak shapes. No peak distortion, nor breakthrough were observed below 10% ACN as injection solvent, resulting in a straight line for

the curve corresponding to 10% ACN (blue curve in Fig. 8). It is worth mentioning that the experimental points beyond an injection volume of 10% V_0 were not represented here because the peak intensity exceeded the UV linearity range. The range of injected volumes resulting in a linear curve gets smaller as the eluent strength of the injection solvent increases. For instance, the linearity can be maintained up to 8% V_0 injected in 30% ACN (black curve), while 3% V_0 in 90% ACN (purple curve). A very clear break occurs in the curve beyond a certain injected volume which fully depends on the injection solvent. This loss of linearity is a fair indicator of the emergence of breakthrough phenomena. This broken curve is followed by a transition zone with a downward curve, and again a growing straight line. The starting point of this straight line is the critical injection volume above which total breakthrough exists. Part of the sample being lost in the dead volume (breakthrough), the peak area starts to decrease with increasing injection volumes. However, above a certain injection volume there is a reversed trend, with peak areas increasing again according to a straight line with a gentle slope. The fact that the peak area increases with the injection volume in total breakthrough conditions is very attractive, because it suggests that larger injection volumes in ^{2}D could lead to better detection sensitivity despite breakthrough. As shown in Fig. 8, this critical volume depends on the injection solvent. Conditions of total breakthrough are reached with lower injection volumes in strong solvents compared to weaker solvents and/or for early eluting peptides. They could be reached with 3% V_0 for peptide #4 (C_e of 16% ACN) in a sample solvent containing 90% ACN, but only 0.5% V_0 for the less retained peptide #6 (C_e of 6% ACN, see Supplementary Information S6). Overall, this study led to surprising conclusions: (i) the breakthrough phenomena can hardly be avoided in ^{2}D-RPLC since it may appear below 0.5% V_0 injected depending on the compound, (ii) total breakthrough could be a good option to maintain good peak shapes in ^{2}D, and (iii) peak area increases linearly with the injected volume beyond the critical injection volume, the slope of the regression line increasing by decreasing the percentage of ACN in the injection solvent.

Accordingly, an alternative approach to circumvent the deleterious impact of injection effects on the separation can consist in injecting a sufficiently large volume in ^{2}D in order to ensure total breakthrough conditions for all peptides. Such strategy might seem counter-intuitive, but based on these observations, it should allow to maximize the peak capacity and the peak intensity in ^{2}D. In order to challenge this new strategy, both repeatability and intermediate precision were evaluated from twelve successive injections and from three successive duplicate injections repeated over five days, respectively. The relative standard deviations calculated for the retention time, the peak intensity, and the peak area for both the breakthrough peak and the retained peak were found to be always below 3%. In addition, the variation of the retained peak area with the peptide concentration (from 5 to 500 mg/L) was quite linear (Fig. 9) with a determination coefficient of 0.999. Furthermore,

the relative standard deviations calculated for each concentration on three successive injections was always below 2%. A good linearity is of prime importance in quantitative LC x LC. Our results suggests that the phenomenon of total breakthrough is not dependent on the solute concentration and hence, that the same proportion of analytes elutes in the dead volume regardless of the analyte concentration. This is important in LC x LC because if injection effects were different depending on the fraction concentration, quantitative analysis would be impossible as well as 2D-reconstruction. We therefore found these results very attractive. They confirm that an approach based on total breakthrough can be used in HILIC x RPLC. Furthermore, they show that the existence of breakthrough leaves open future perspectives in quantitative analysis.

3.2. Application to on-line HILIC x RPLC-UV-HRMS analysis of a tryptic digest

Once the above conditions selected, the on-line HILIC x RPLC method was optimized according to a previously described procedure [6,7]. This procedure relies on the combined use of predictive calculations and Pareto-optimality approach to optimize the physical parameters impacting the quality of the 2D separation. The optimized parameters included the ^{1}D flow rate, the sampling rate, and the split ratio between both dimensions. Our objective was to separate a tryptic digest of 6 proteins in 30 min, using HRMS detection. In order to test our total breakthrough strategy, three different split ratios between ^{1}D and ^{2}D were considered (i.e. no split, split 1:1 and split 1:3), leading to ^{2}D injected volumes of about 28%, 14%, and 7% V_0, respectively. The operating conditions are given in Table 3.

Fig. 10 shows extracted ion chromatograms (EIC) corresponding to one strongly retained peptide in ^{2}D-RPLC. Three analyses of the tryptic digest were carried out in HILIC x RPLC-UV-HRMS with three different split ratios between both dimensions (no split, 1:1 and 1:3). The peptide was retained in ^{1}D-HILIC with an elution composition, and hence an injection solvent in ^{2}D-RPLC, close to 75 % ACN. Considering the elution composition of this peptide in ^{2}D-RPLC (40% ACN), it was affected by a breakthrough phenomenon with a peak of breakthrough indicated by an asterisk in Figs.10a to 10c. The peak shape is very bad with 1:1 and 1:3 as split ratios (5 and 10 µL injected, respectively) while good with no split (20 µL injected). In this example, the critical injection volume (required to be in conditions of total breakthrough) was found to be between 10 and 20 µL. Similarly, 20 µL was found to be above the critical injection volume for all peptides, suggesting that any injected volume higher than 20 µL was suitable.

Figs.11a shows the 3D-chromatogram of the tryptic digest obtained without split in on-line HILIC x RPLC-UV-HRMS analysis. For the purpose of clarity, only the separation area is represented. The

entire 2D-contour plot can be seen in Supplementary Information S7. As can be observed in Fig. 11a, the 2D-separation is totally orthogonal, with a calculated retention space coverage (γ) close to 1. Peaks appear to be very narrow and symmetrical. The performance of this optimized on-line HILIC x RPLC separation was evaluated in term of peak capacity by taking into account the retention space coverage, the under-sampling and the average peak width in each dimension according to Eq.8. All the experimental results are given in Table 4. Due to the matrix complexity, ^{1}D peak widths were measured from ten representative standards injected in similar chromatographic conditions. ^{2}D peak widths were measured from more than hundred peaks eluted all along the chromatogram. An effective peak capacity of 1500 was found for this separation achieved in 30 min, which is quite impressive compared to what was obtained in RPLC x RPLC within the same time [43]. For more objective comparative purposes, the same sample was analysed in on-line RPLC x RPLC under optimized conditions considering the same gradient time of 30 min. The operating conditions are given in Table 3 and the resulting separation is shown in Fig.11b. The first observation that can be made is that an average 5-fold lower peak height was obtained in HILIC x RPLC (Fig.11a) compared to RPLC x RPLC (Fig.11b). As previously discussed, the benefit of having RPLC in ^{1}D is that large volumes of undiluted aqueous sample could be injected without peak distortion (12% V_0 in RPLC vs. 5% V_0 in HILIC). The lower peak height in HILIC x RPLC compared to RPLC x RPLC is thus both due to the lower injected amount in ^{1}D and to the omnipresence of breakthrough phenomenon in ^{2}D. However, as expected with such combination, the retention space coverage was incomplete in RPLC x RPLC with a peak distribution around the diagonal of the separation space. Consequently, the effective peak capacity was found to be 830 despite the good peak shapes in ^{2}D. The HILIC x RPLC separation resulted in an increase in peak capacity of about 80% compared to RPLC x RPLC. Such an increase can be ascribed to the full retention space coverage with quite symmetrical peaks. Regarding HILIC x RPLC, It should be emphasized that the presence of only one symmetrical retained peak in ^{2}D despite breakthrough was systematically verified by EIC-HRMS for every expected peptides. Fig. 12a shows the 2D-contour plot obtained in HILIC x RPLC-UV. In the latter, nine spots labelled from #1 to #9 and corresponding to nine peptide peaks distributed throughout the 2D-separation space are highlighted. The peaks #1 to #3 are strongly retained in HILIC while the peaks #7 to #9 are poorly retained. Similarly, the peaks #1, #4, and #7 are poorly retained in RPLC while the peaks #3, #6, and #9 are strongly retained. The peak #5 is eluted in the middle of the retention space. The nine corresponding EIC-HRMS are shown in Fig.12b. It is very interesting to note that all the retained peaks are quite symmetrical and that no additional peak appears aside from the unretained peak of breakthrough. As expected the ratio of peak areas between breakthrough and retained peaks depends on the peptide retention in both ^{1}D and ^{2}D. As above discussed, weakly retained peptides in

609 ^{2}D are more impacted by breakthrough phenomena, especially when they are poorly retained in ^{1}D
610 (strong injection solvent). It is therefore important to note that for good quantitative performance,
611 the internal standard has to be eluted in the same retention conditions as the compound of interest.
612 However, the separations shown in Fig.12 confirm that an injection volume of 20 µL was sufficient to
613 ensure total breakthrough for all peptides and demonstrate the validity of the proposed approach
614 for HILIC x RPLC separations.
615
616 **4. Conclusion**
617
618 We have developed an on-line HILIC x RPLC-UV-HRMS method for the comprehensive
619 characterization of a protein digest in 30 min.
620 In the first dimension, the stationary phase and the injection conditions were deeply studied and
621 carefully selected to find the best trade-off between high peak capacity, and low dilution. Bare silicas
622 were found to be the most appropriate stationary phases for the separation of peptides under
623 neutral pH with ammonium acetate as additive. The use of HILIC in the first dimension raised the
624 issue of finding an adequate sample solvent with respect to both sample solubility and injection
625 effects. It was shown that a minimum of 50% water was required in the injection solvent for proper
626 peptide dissolution.
627 The high percentage of acetonitrile in the HILIC-mobile phase, and hence in the injection solvent for
628 RPLC may lead to peak broadening, peak distortion and breakthrough phenomena, resulting in a
629 dramatic loss of peak capacity and peak intensity. The conditions of emergence of peak broadening
630 and peak distortion were deeply investigated. The importance of both the injection volume and the
631 difference in composition between injection and elution solvents were highlighted. Although limiting
632 the injection volume is the most obvious approach to avoid injection effects, we discovered that
633 injecting large volumes offers a powerful alternative approach. Our results proved that above a
634 certain critical injection volume, depending on the elution conditions, narrow and symmetrical peaks
635 can be obtained for peptides, despite the persistence of breakthrough. This counter-intuitive “total
636 breakthrough” approach was applied for the on-line HILIC x RPLC-UV-HRMS analysis of a complex
637 tryptic digest sample. Due both to the high retention space coverage and to the sharp peaks
638 obtained in the second dimension, a peak capacity close to 1500 could be achieved in 30 minutes.
639 Within the same analysis time of 30 min and under optimized conditions, the obtained peak capacity
640 in RPLC x RPLC was half as high, and the average peak intensity was about 5-fold higher.
641 Nonetheless, this work shows the great potential of on-line HILIC x RPLC performed under “total
642 breakthrough” conditions for the ultra-fast 2D-separation of complex peptide samples.

Acknowledgements

The authors warmly thank Agilent Technologies for the loan of the 2D-LC instrument and the QTOF-HRMS. They also would like to thank Professor Gert Desmet and Vincent Pepermans from the University of Brussels for stimulating discussions.

Figure captions

Figure 1: Influence of the injection solvent on the peak shape of two peptides in HILIC: (a) peptide #4 with 1.2 µL (1% V_0) injected, and (b) peptide #8 with 12 µL (10% V_0) injected, both at a concentration of 42 mg/L. Injection solvent compositions: : 0:100 (red), 25:75 (black), 50:50 (green) or 75:25 (blue) ACN/water (v/v). Acquity BEH Amide (50 mm x 2.1 mm, 1.7 µm) column, 30 °C, 0.6 mL/min, A: ACN and B: 10 mM ammonium acetate in water, 2-60% B in 29 t_0. UV detection at 210 nm.

Figure 2: Comparison of peak shapes of (a) peptide #4 and (b) peptide #8 obtained in HILIC by injecting a constant amount of peptides with different injection volumes and different injection solvents resulting in different dilution with ACN: 1.2 µL (1% V_0) in 0:100 ACN/water (42 mg/L, no dilution) (red), 2.4 µL (2% V_0) in 50:50 ACN/water (21 mg/L, 2-fold dilution) (green), 4.8µL (4% V_0) in 75:25 ACN/water (10.5 mg/L, 4-fold dilution) (blue), and 12µL (10% V_0) in 90:10 ACN/water (4.2 mg/L, 10-fold dilution) (black). Other conditions as in Fig.1.

Figure 3: Overlaid HILIC separations of a constant amount of protein tryptic digest with different injection volumes and different injection solvents resulting in different dilution with ACN : 2 µL (1.7% V_0) in 0:100 ACN/water (no dilution) (red), 4 µL (3.3% V_0) in 50:50 ACN/water (2-fold dilution) (green), 8 µL (6.6% V_0) in 75:25 ACN/water (4-fold dilution) (blue), and 20 µL (16% V_0) in 90:10 ACN/water (10-fold dilution) (black). Column Acquity BEH HILIC (50 mm x 2.1 mm, 1.7 µm), 30°C, 0.5 mL/min, A: ACN, B: 10 mM ammonium acetate in water, 13-52% B in 9.7 t_0. UV detection at 210 nm.

Figure 4: Separations of a tryptic digest of 6 proteins in HILIC with 10 different stationary phases: (a) Hypersil HILIC (#1), (b) Acquity BEH HILIC (#2), (c) Acquity amide (#3), (d) Hypersil Gold HILIC (#4), (e) Nucleodur HILIC (#5), (f) Kinetex HILIC (#6), (g) Nucleoshell HILIC (#7), (h) Accucore HILIC (#8), (i) Luna NH2 (#9), and (j) Cortecs HILIC (#10). 5% V_0 injected in 50:50 ACN/water (v/v) (2-fold dilution). Column characteristics, associated flow-rates, and gradient times are listed in Table 2. Other conditions are given in experimental section.

Figure 5: Overlaid peaks of peptide #4 obtained in RPLC with different injection volumes (0.5, 1, and 3 µL) emphasizing the impact of solute concentration: (a) 16 mg/L vs. (b) 80 mg/L, both in 30:70 water/ACN (v/v). Kinetex C18 (30 mm x 2.1 mm, 1.3 µm) column, A: water with formic acid (0.1%), B: ACN with formic acid (0.1%), 1-45% B in 5.5 t_0. Other conditions given in the experimental section.

Figure 6: Overlaid peaks of peptide #4 (80 mg/L in 30:70 water/ACN (v/v)) obtained in RPLC with different injection volumes (1%, 2%, and 6% V_0) emphasizing the impact of the nature of the stationary phase: (a) Kinetex C18 (30 mm x 2.1 mm, 1.3 µm), and (b) Acquity CSH C18 (30 mm x 2.1 mm, 1.7 µm), 1-45% B in 44 t_0. Other conditions as in Fig. 5.

Figure 7: Evolution of the peak shapes of peptide #4 (50 mg/L in 50:50 water/ACN) with increasing injection volumes: (a) 1 µL (1.5% V_0), (b) 1.5 µL (2.1% V_0), (c) 1.8 µL (2.5% V_0), (d) 2.2 µL (3% V_0), (e) 3.5 µL (4.8% V_0), and (f) 4.5 µL (6.2% V_0). 1-45% B in 11.3 t_0, 80°C, 1.5 mL/min. MS detection ESI+ (EIC 557.6). Other conditions given in experimental section. The asterisk indicates the peak of breakthrough.

Figure 8: Variation of the peak area (peptide #4) with the ratio of the injection volume to the column dead volume ($V_{injected}/V_0$). Injection solvent: 10% ACN (blue), 30% ACN (black) 50% ACN (red), 70% ACN (green) or 90% ACN (purple) in water. UV detection at 210 nm. Same other conditions as in Fig. 7.

Figure 9: Variation of the peak area with the concentration (peptide #4) in conditions of « total breakthrough ». Injection solvent 30:70 water/ACN (v/v), 3.5 µL (4.8% V_0) injected. UV detection at 210 nm. Other conditions as in Fig.7.

Figure 10: Extracted ion chromatograms (EIC 742.4536) in ^{2}D of one fraction in HILIC x RPLC–HRMS. Sample: tryptic digest of 6 proteins. Split ratio between both dimensions: (a) no split (20 µL injected), (b) split 1:1 (10 µL injected), and (c) split 1:3 (5 µL injected). The fraction was injected in nearly 75% ACN. MS detection ESI+. Other conditions are given in Table 3.

Figure 11: 3D-chromatograms obtained for the separation of a tryptic digest of 6 proteins in (a) on-line HILIC x RPLC (without split), and (b)) on-line RPLC x RPLC (split 1:2). UV detection at 210 nm. Conditions are given in Table 3.

Figure 12: On-line HILIC x RPLC-UV-HRMS analysis of a tryptic digest of 6 proteins. (a) 2D-contour plot with UV detection at 210 nm and (b) RPLC-EIC-HRMS of 9 different fractions (#1 to #9) with m/z 650.3160 (#1), 1013.6004 (#2), 288.2907 (#3), 748.3117 (#4), 1023.5553 (#5), 1557.3651 (#6),

803.9448 (#7), 689.9255 (#8), and 1585.8743 (#9). The corresponding retained peaks are indicated by black spots in the 2D-contour plot. Conditions are given in Table 3.

References

[1] K. Horváth, J.N. Fairchild, G. Guiochon, Generation and Limitations of Peak Capacity in Online Two-Dimensional Liquid Chromatography, Anal. Chem. 81 (2009) 3879–3888. https://doi.org/10.1021/ac802694c.

[2] M. Sarrut, G. Crétier, S. Heinisch, Theoretical and practical interest in UHPLC technology for 2D-LC, TrAC Trends in Analytical Chemistry. 63 (2014) 104–112. https://doi.org/10.1016/j.trac.2014.08.005.

[3] F. Bedani, P.J. Schoenmakers, H.-G. Janssen, Theories to support method development in comprehensive two-dimensional liquid chromatography – A review, J. Sep. Science. 35 (2012) 1697–1711. https://doi.org/10.1002/jssc.201200070.

[4] X. Li, D.R. Stoll, P.W. Carr, Equation for Peak Capacity Estimation in Two-Dimensional Liquid Chromatography, Anal. Chem. 81 (2009) 845–850. https://doi.org/10.1021/ac801772u.

[5] I. François, D. Cabooter, K. Sandra, F. Lynen, G. Desmet, P. Sandra, Tryptic digest analysis by comprehensive reversed phase×two reversed phase liquid chromatography (RP-LC×2RP-LC) at different pH's, J. Sep. Science. 32 (2009) 1137–1144. https://doi.org/10.1002/jssc.200800578.

[6] M. Sarrut, A. D'Attoma, S. Heinisch, Optimization of conditions in on-line comprehensive two-dimensional reversed phase liquid chromatography. Experimental comparison with one-dimensional reversed phase liquid chromatography for the separation of peptides, Journal of Chromatography A. 1421 (2015) 48–59. https://doi.org/10.1016/j.chroma.2015.08.052.

[7] A. D'Attoma, S. Heinisch, On-line comprehensive two dimensional separations of charged compounds using reversed-phase high performance liquid chromatography and hydrophilic interaction chromatography. Part II: Application to the separation of peptides, Journal of Chromatography A. 1306 (2013) 27–36. https://doi.org/10.1016/j.chroma.2013.07.048.

[8] A. D'Attoma, C. Grivel, S. Heinisch, On-line comprehensive two-dimensional separations of charged compounds using reversed-phase high performance liquid chromatography and hydrophilic interaction chromatography. Part I: Orthogonality and practical peak capacity considerations, Journal of Chromatography A. 1262 (2012) 148–159. https://doi.org/10.1016/j.chroma.2012.09.028.

[9] G. Vanhoenacker, I. Vandenheede, F. David, P. Sandra, K. Sandra, Comprehensive two-dimensional liquid chromatography of therapeutic monoclonal antibody digests, Anal Bioanal Chem. 407 (2015) 355–366. https://doi.org/10.1007/s00216-014-8299-1.

[10] K. Horie, Y. Sato, T. Kimura, T. Nakamura, Y. Ishihama, Y. Oda, T. Ikegami, N. Tanaka, Estimation and optimization of the peak capacity of one-dimensional gradient high performance liquid chromatography using a long monolithic silica capillary column, Journal of Chromatography A. 1228 (2012) 283–291. https://doi.org/10.1016/j.chroma.2011.12.088.

[11] M. Gilar, P. Olivova, A.E. Daly, J.C. Gebler, Orthogonality of Separation in Two-Dimensional Liquid Chromatography, Anal. Chem. 77 (2005) 6426–6434. https://doi.org/10.1021/ac050923i.

[12] P.G. Stevenson, D.N. Bassanese, X.A. Conlan, N.W. Barnett, Improving peak shapes with counter gradients in two-dimensional high performance liquid chromatography, Journal of Chromatography A. 1337 (2014) 147–154. https://doi.org/10.1016/j.chroma.2014.02.051.

[13] Y. Chen, J. Li, O.J. Schmitz, Development of an At-Column Dilution Modulator for Flexible and Precise Control of Dilution Factors to Overcome Mobile Phase Incompatibility in Comprehensive Two-Dimensional Liquid Chromatography, Anal. Chem. 91 (2019) 10251–10257. https://doi.org/10.1021/acs.analchem.9b02391.

[14] D.R. Stoll, D.C. Harmes, G.O. Staples, O.G. Potter, C.T. Dammann, D. Guillarme, A. Beck, Development of Comprehensive Online Two-Dimensional Liquid Chromatography/Mass Spectrometry Using Hydrophilic Interaction and Reversed-Phase Separations for Rapid and Deep Profiling of Therapeutic Antibodies, Anal. Chem. 90 (2018) 5923–5929. https://doi.org/10.1021/acs.analchem.8b00776.

[15] L. Montero, M. Herrero, E. Ibáñez, A. Cifuentes, Separation and characterization of phlorotannins from brown algae Cystoseira abies-marina by comprehensive two-dimensional liquid chromatography, ELECTROPHORESIS. 35 (2014) 1644–1651. https://doi.org/10.1002/elps.201400133.

[16] C.M. Willemse, M.A. Stander, A.G.J. Tredoux, A. de Villiers, Comprehensive two-dimensional liquid chromatographic analysis of anthocyanins, Journal of Chromatography A. 1359 (2014) 189–201. https://doi.org/10.1016/j.chroma.2014.07.044.

[17] X.-X. Zheng, Y. Du, B. Xu, T. Wang, Q. Zhong, Z. Li, S. Ji, M. Guo, D. Yang, D. Tang, Off-line two-dimensional liquid chromatography coupled with diode array detection and quadrupole-time of flight mass spectrometry for the biotransformation kinetics of Ginkgo biloba leaves extract by diabetic rat liver microsomes, Journal of Chromatography B. 1109 (2019) 1–9. https://doi.org/10.1016/j.jchromb.2019.01.015.

[18] V. Elsner, V. Wulf, M. Wirtz, O.J. Schmitz, Reproducibility of retention time and peak area in comprehensive two-dimensional liquid chromatography, Anal Bioanal Chem. 407 (2015) 279–284. https://doi.org/10.1007/s00216-014-8090-3.

[19] S. Abrar, B. Trathnigg, Separation of nonionic surfactants according to functionality by hydrophilic interaction chromatography and comprehensive two-dimensional liquid chromatography, Journal of Chromatography A. 1217 (2010) 8222–8229. https://doi.org/10.1016/j.chroma.2010.10.118.

[20] A.F.G. Gargano, M. Duffin, P. Navarro, P.J. Schoenmakers, Reducing Dilution and Analysis Time in Online Comprehensive Two-Dimensional Liquid Chromatography by Active Modulation, Anal. Chem. 88 (2016) 1785–1793. https://doi.org/10.1021/acs.analchem.5b04051.

[21] L. Montero, E. Ibáñez, M. Russo, R. di Sanzo, L. Rastrelli, A.L. Piccinelli, R. Celano, A. Cifuentes, M. Herrero, Metabolite profiling of licorice (Glycyrrhiza glabra) from different locations using comprehensive two-dimensional liquid chromatography coupled to diode array and tandem mass spectrometry detection, Analytica Chimica Acta. 913 (2016) 145–159. https://doi.org/10.1016/j.aca.2016.01.040.

[22] E. Sommella, O.H. Ismail, F. Pagano, G. Pepe, C. Ostacolo, G. Mazzoccanti, M. Russo, E. Novellino, F. Gasparrini, P. Campiglia, Development of an improved online comprehensive hydrophilic interaction chromatography × reversed-phase ultra-high-pressure liquid chromatography platform for complex multiclass polyphenolic sample analysis, J. Sep. Sci. 40 (2017) 2188–2197. https://doi.org/10.1002/jssc.201700134.

[23] L. Montero, V. Sáez, D. von Baer, A. Cifuentes, M. Herrero, Profiling of Vitis vinifera L. canes (poly)phenolic compounds using comprehensive two-dimensional liquid

chromatography, Journal of Chromatography A. 1536 (2018) 205–215. https://doi.org/10.1016/j.chroma.2017.06.013.

[24] P. Donato, F. Rigano, F. Cacciola, M. Schure, S. Farnetti, M. Russo, P. Dugo, L. Mondello, Comprehensive two-dimensional liquid chromatography–tandem mass spectrometry for the simultaneous determination of wine polyphenols and target contaminants, Journal of Chromatography A. 1458 (2016) 54–62. https://doi.org/10.1016/j.chroma.2016.06.042.

[25] P. Jandera, T. Hájek, Z. Šromová, Comprehensive two-dimensional monolithic liquid chromatography of polar compounds, Journal of Separation Science. 42 (2019) 670–677. https://doi.org/10.1002/jssc.201801085.

[26] M. Muller, A.G.J. Tredoux, A. de Villiers, Application of Kinetically Optimised Online HILIC × RP-LC Methods Hyphenated to High Resolution MS for the Analysis of Natural Phenolics, Chromatographia. 82 (2019) 181–196. https://doi.org/10.1007/s10337-018-3662-6.

[27] R. Berkecz, F. Tömösi, T. Körmöczi, V. Szegedi, J. Horváth, T. Janáky, Comprehensive phospholipid and sphingomyelin profiling of different brain regions in mouse model of anxiety disorder using online two-dimensional (HILIC/RP)-LC/MS method, Journal of Pharmaceutical and Biomedical Analysis. 149 (2018) 308–317. https://doi.org/10.1016/j.jpba.2017.10.043.

[28] H. Zhang, J.-M. Jiang, D. Zheng, M. Yuan, Z.-Y. Wang, H.-M. Zhang, C.-W. Zheng, L.-B. Xiao, H.-X. Xu, A multidimensional analytical approach based on time-decoupled online comprehensive two-dimensional liquid chromatography coupled with ion mobility quadrupole time-of-flight mass spectrometry for the analysis of ginsenosides from white and red ginsengs, Journal of Pharmaceutical and Biomedical Analysis. 163 (2019) 24–33. https://doi.org/10.1016/j.jpba.2018.09.036.

[29] J.-L. Cao, L.-J. Ma, S.-P. Wang, Y. Deng, Y.-T. Wang, P. Li, J.-B. Wan, Comprehensively qualitative and quantitative analysis of ginsenosides in Panax notoginseng leaves by online two-dimensional liquid chromatography coupled to hybrid linear ion trap Orbitrap mass spectrometry with deeply optimized dilution and modulation system, Analytica Chimica Acta. 1079 (2019) 237–251. https://doi.org/10.1016/j.aca.2019.06.040.

[30] D.V. McCalley, A study of column equilibration time in hydrophilic interaction chromatography, Journal of Chromatography A. 1554 (2018) 61–70. https://doi.org/10.1016/j.chroma.2018.04.016.

[31] M. Muller, A.G.J. Tredoux, A. de Villiers, Predictive kinetic optimisation of hydrophilic interaction chromatography × reversed phase liquid chromatography separations: Experimental verification and application to phenolic analysis, Journal of Chromatography A. 1571 (2018) 107–120. https://doi.org/10.1016/j.chroma.2018.08.004.

[32] T. Hájek, P. Jandera, M. Staňková, P. Česla, Automated dual two-dimensional liquid chromatography approach for fast acquisition of three-dimensional data using combinations of zwitterionic polymethacrylate and silica-based monolithic columns, Journal of Chromatography A. 1446 (2016) 91–102. https://doi.org/10.1016/j.chroma.2016.04.007.

[33] G. Groeneveld, M.N. Dunkle, M. Rinken, A.F.G. Gargano, A. de Niet, M. Pursch, E.P.C. Mes, P.J. Schoenmakers, Characterization of complex polyether polyols using comprehensive two-dimensional liquid chromatography hyphenated to high-resolution mass spectrometry, Journal of Chromatography A. 1569 (2018) 128–138. https://doi.org/10.1016/j.chroma.2018.07.054.

[34] A. Martín-Ortiz, A.I. Ruiz-Matute, M.L. Sanz, F.J. Moreno, M. Herrero, Separation of di- and trisaccharide mixtures by comprehensive two-dimensional liquid chromatography. Application to prebiotic oligosaccharides, Analytica Chimica Acta. 1060 (2019) 125–132. https://doi.org/10.1016/j.aca.2019.01.040.

[35] L.R. Snyder, J.W. Dolan, J.R. Gant, Gradient elution in high-performance liquid chromatography: I. Theoretical basis for reversed-phase systems, Journal of Chromatography A. 165 (1979) 3–30. https://doi.org/10.1016/S0021-9673(00)85726-X.

[36] D.R. Stoll, X. Wang, P.W. Carr, Comparison of the Practical Resolving Power of One- and Two-Dimensional High-Performance Liquid Chromatography Analysis of Metabolomic Samples, Anal. Chem. 80 (2008) 268–278. https://doi.org/10.1021/ac701676b.

[37] B. Chauve, D. Guillarme, P. Cléon, J.-L. Veuthey, Evaluation of various HILIC materials for the fast separation of polar compounds, Journal of Separation Science. 33 (2010) 752–764. https://doi.org/10.1002/jssc.200900749.

[38] Y. Yang, R.I. Boysen, M.T.W. Hearn, Hydrophilic interaction chromatography coupled to electrospray mass spectrometry for the separation of peptides and protein digests, Journal of Chromatography A. 1216 (2009) 5518–5524. https://doi.org/10.1016/j.chroma.2009.05.085.

[39] J. Ruta, S. Rudaz, D.V. McCalley, J.-L. Veuthey, D. Guillarme, A systematic investigation of the effect of sample diluent on peak shape in hydrophilic interaction liquid chromatography, Journal of Chromatography A. 1217 (2010) 8230–8240. https://doi.org/10.1016/j.chroma.2010.10.106.

[40] G.C. Derringer, R.L. Markham, A computer-based methodology for matching polymer structures with required properties, Journal of Applied Polymer Science. 30 (1985) 4609–4617. https://doi.org/10.1002/app.1985.070301208.

[41] S. Heinisch, A. D'Attoma, C. Grivel, Effect of pH additive and column temperature on kinetic performance of two different sub-2µm stationary phases for ultrafast separation of charged analytes, Journal of Chromatography A. 1228 (2012) 135–147. https://doi.org/10.1016/j.chroma.2011.08.041.

[42] D.V. McCalley, Overload for Ionized Solutes in Reversed-Phase High-Performance Liquid Chromatography, Analytical Chemistry. 78 (2006) 2532–2538. https://doi.org/10.1021/ac052098b.

[43] M. Sarrut, F. Rouvière, S. Heinisch, Theoretical and experimental comparison of one dimensional versus on-line comprehensive two dimensional liquid chromatography for optimized sub-hour separations of complex peptide samples, Journal of Chromatography A. 1498 (2017) 183–195. https://doi.org/10.1016/j.chroma.2017.01.054.

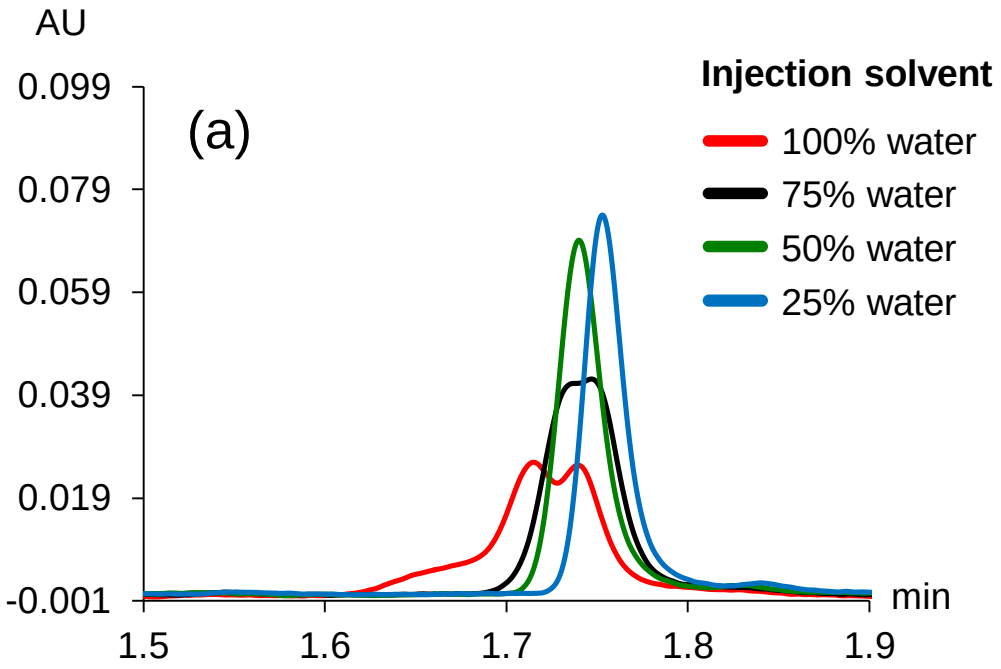
AU
0.099
0.079
0.059
0.039
0.019
-0.001
(a)
Injection solvent
100% water
75% water
50% water
25% water
min
1.5
1.6
1.7
1.8
1.9

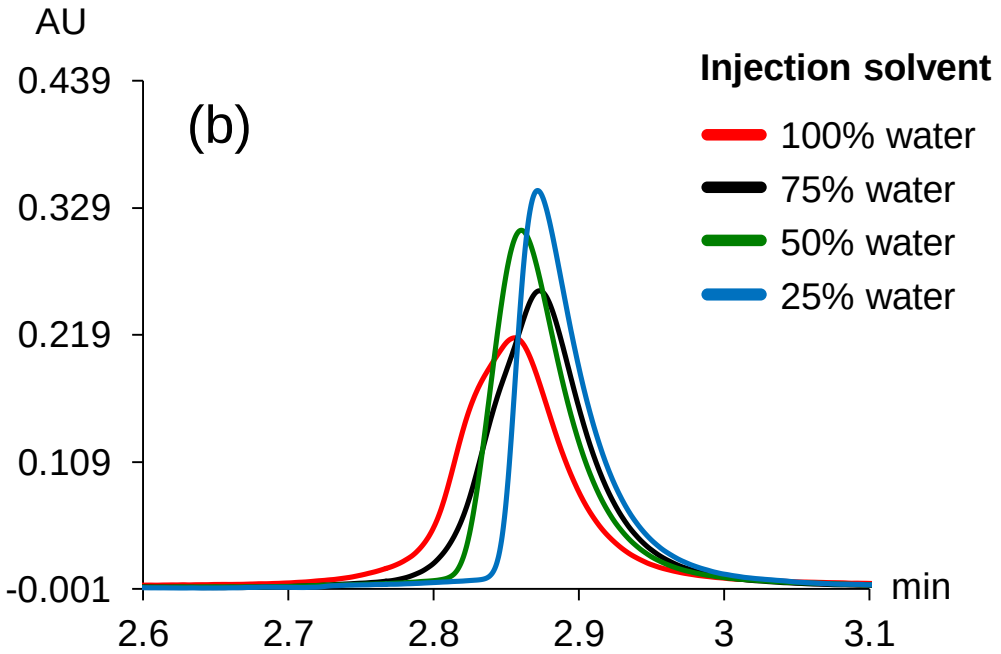
AU
0.439
0.329
0.219
0.109
-0.001
(b)
Injection solvent
100% water
75% water
50% water
25% water
min
2.6
2.7
2.8
2.9
3
3.1

Figure 1

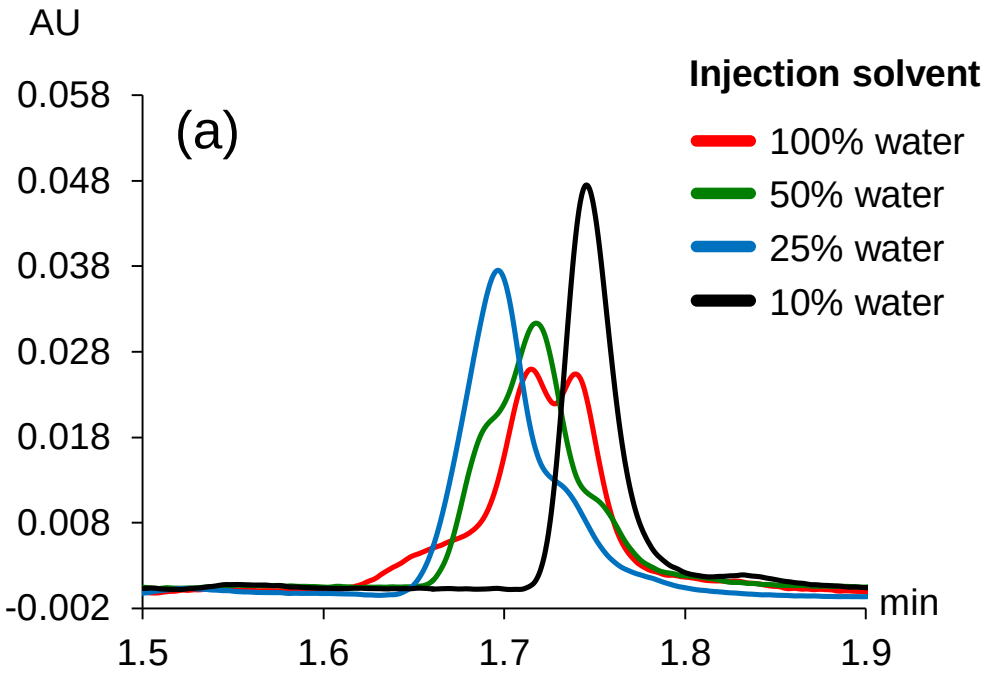
AU
(a)
Injection solvent
100% water
50% water
25% water
10% water
0.058
0.048
0.038
0.028
0.018
0.008
-0.002
min
1.5
1.6
1.7
1.8
1.9

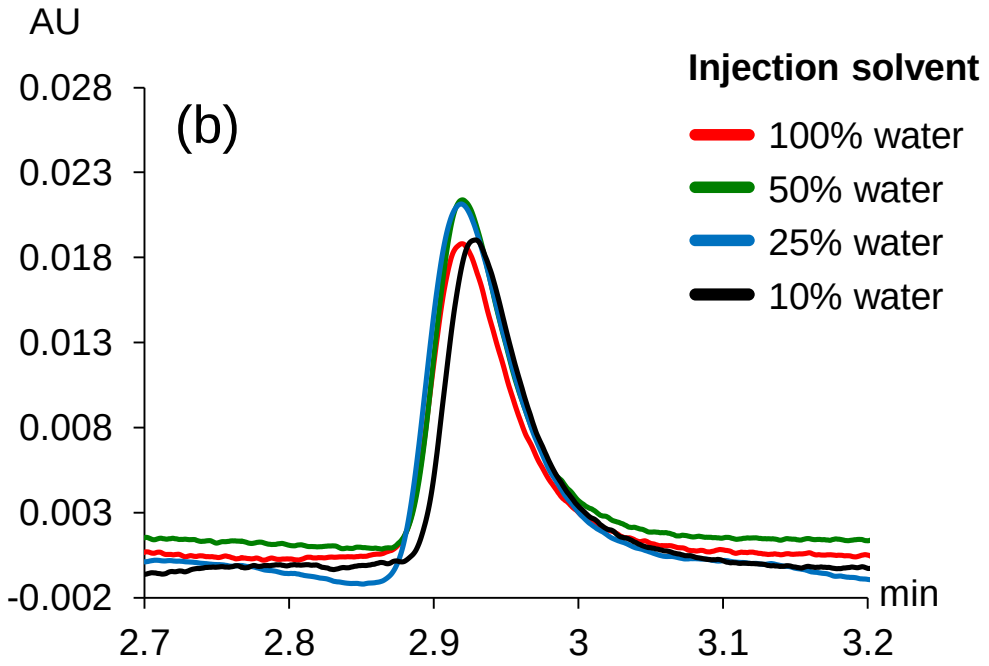
AU
(b)
Injection solvent
100% water
50% water
25% water
10% water
0.028
0.023
0.018
0.013
0.008
0.003
-0.002
min
2.7
2.8
2.9
3
3.1
3.2

Figure 2

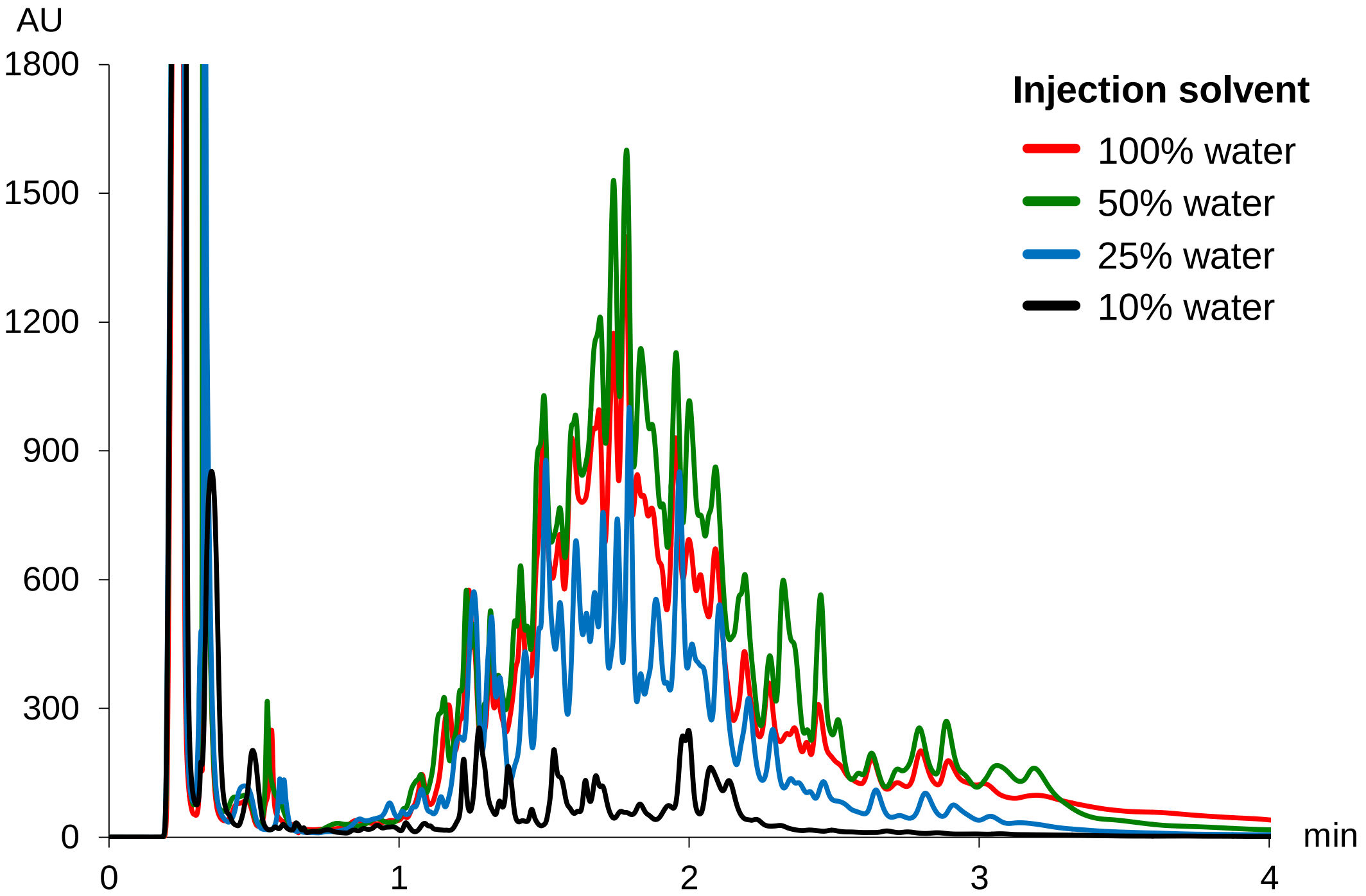
AU
1800
1500
1200
900
600
300
0
0
1
2
3
4
min
Injection solvent
100% water
50% water
25% water
10% water

Figure 3

Figure 4

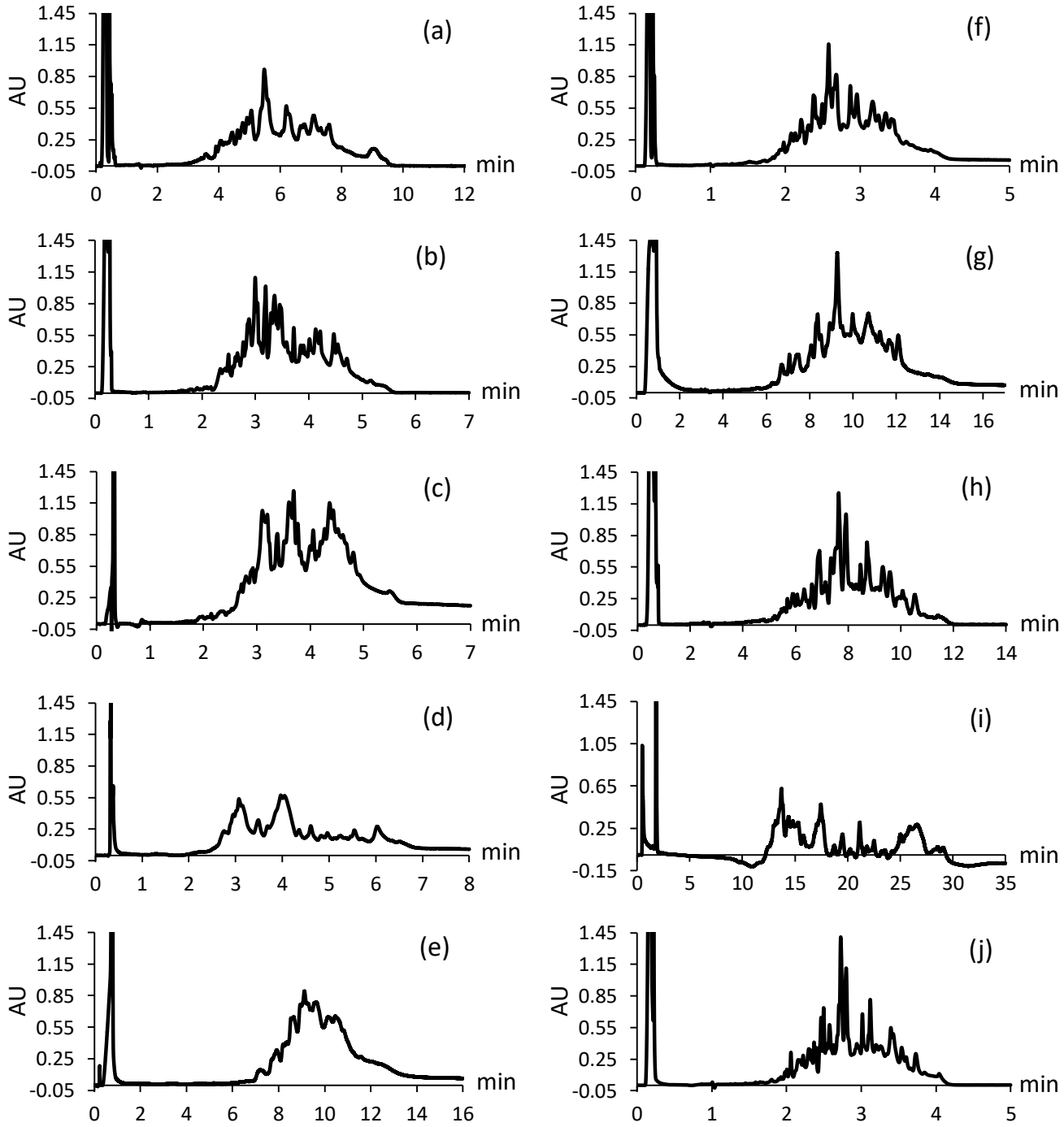

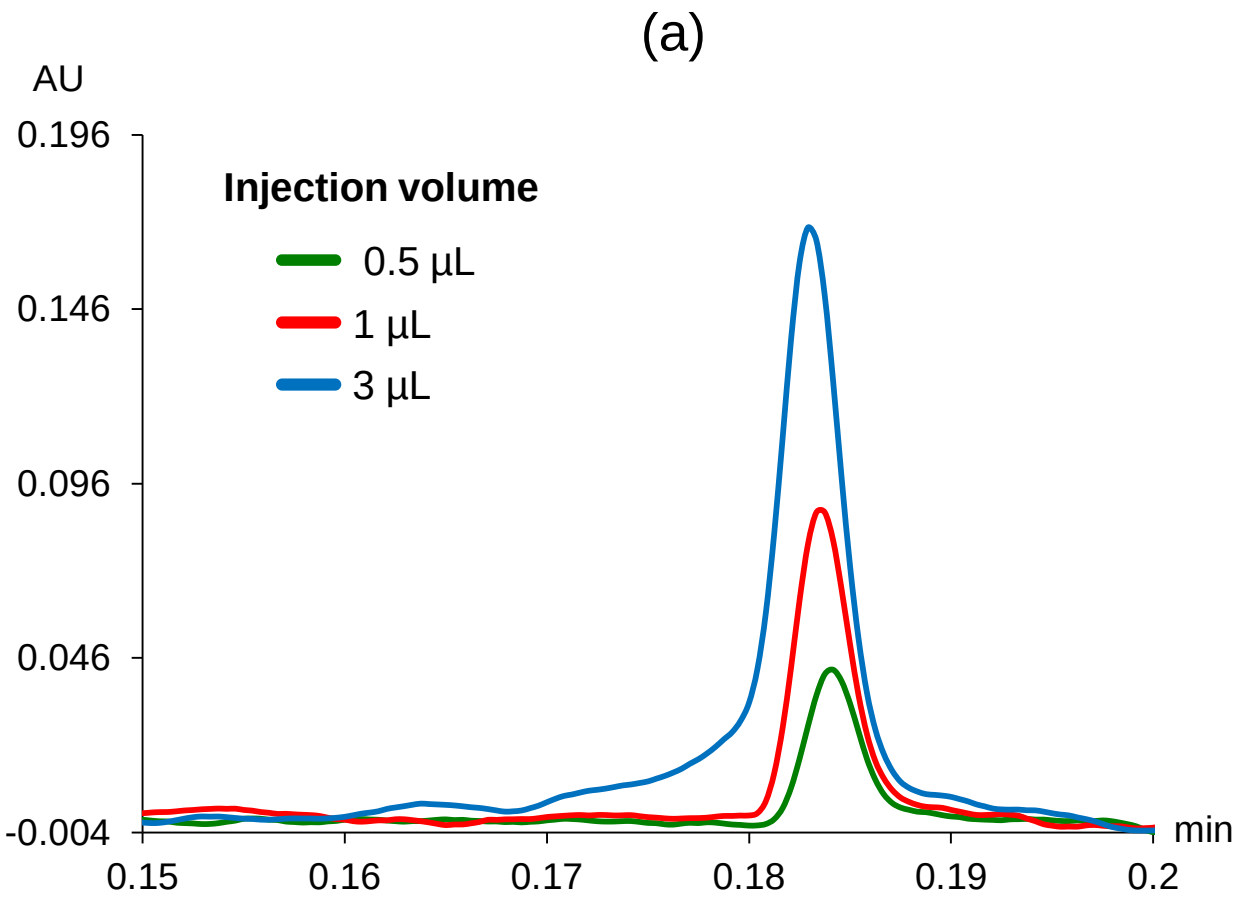
(a)
AU
0.196
0.146
0.096
0.046
-0.004
Injection volume
0.5 µL
1 µL
3 µL
0.15
0.16
0.17
0.18
0.19
0.2
min

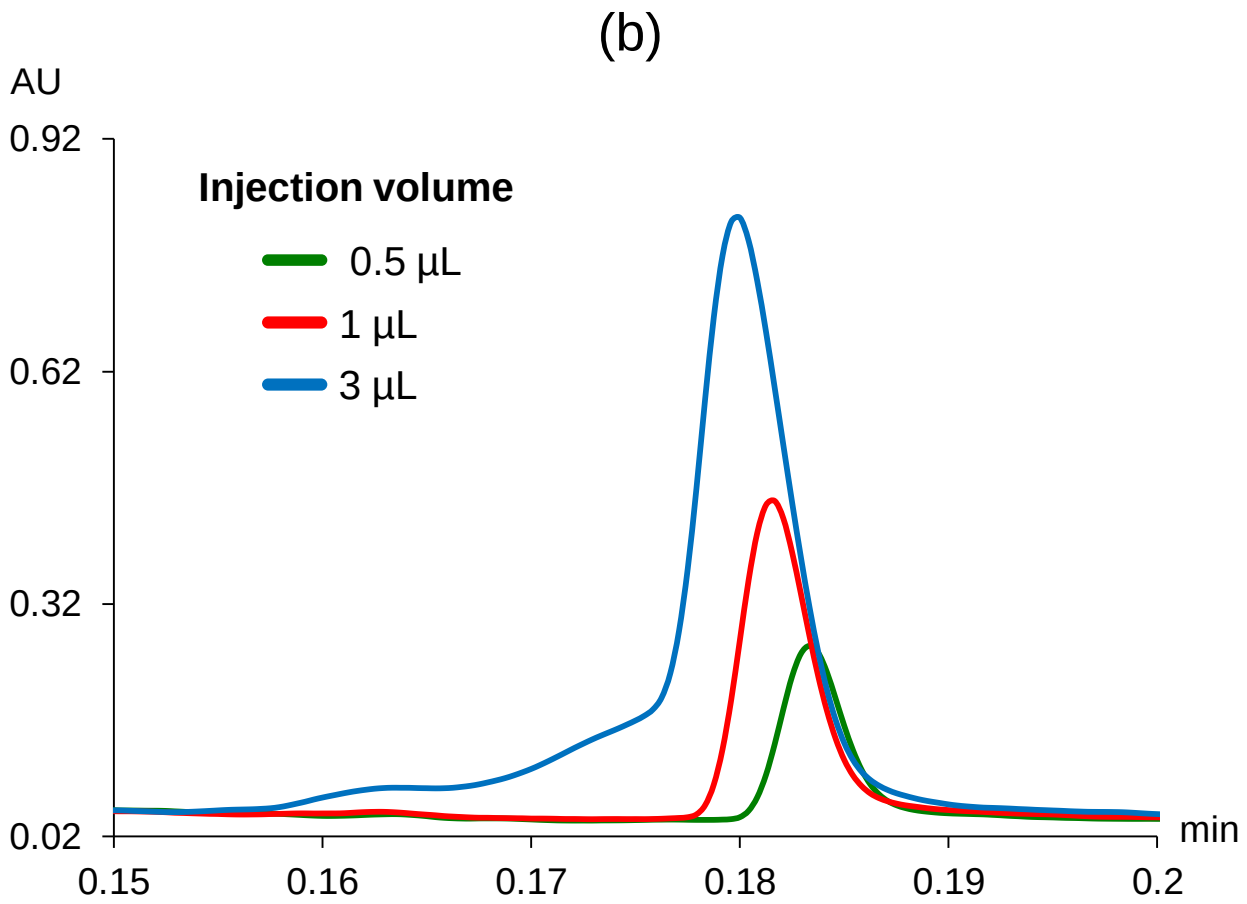
(b)
AU
0.92
0.62
0.32
0.02
Injection volume
0.5 µL
1 µL
3 µL
0.15
0.16
0.17
0.18
0.19
0.2
min

Figure 5

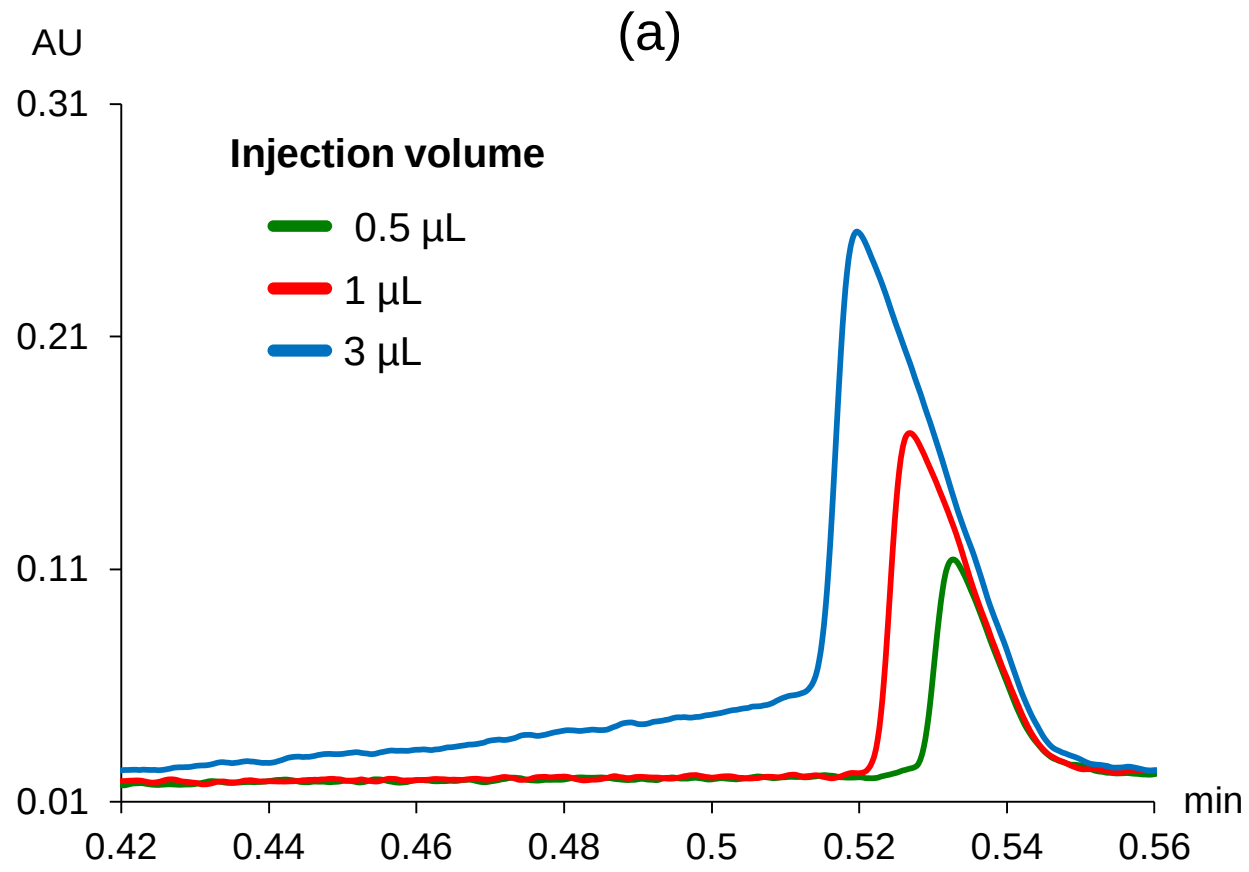
(a)
AU
0.31
0.21
0.11
0.01
Injection volume
0.5 µL
1 µL
3 µL
0.42
0.44
0.46
0.48
0.5
0.52
0.54
0.56
min

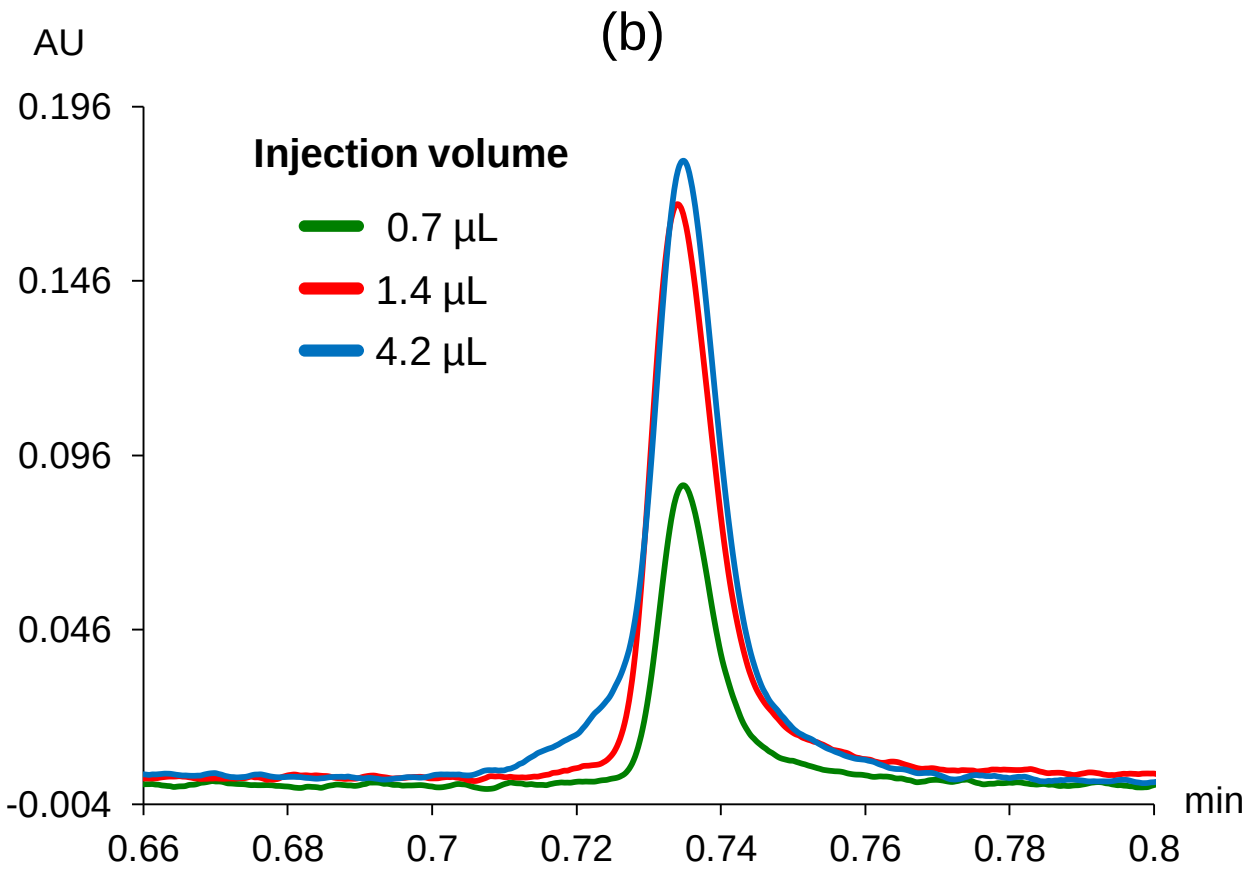
(b)
AU
0.196
0.146
0.096
0.046
-0.004
Injection volume
0.7 µL
1.4 µL
4.2 µL
0.66
0.68
0.7
0.72
0.74
0.76
0.78
0.8
min

Figure 6

Figure 7

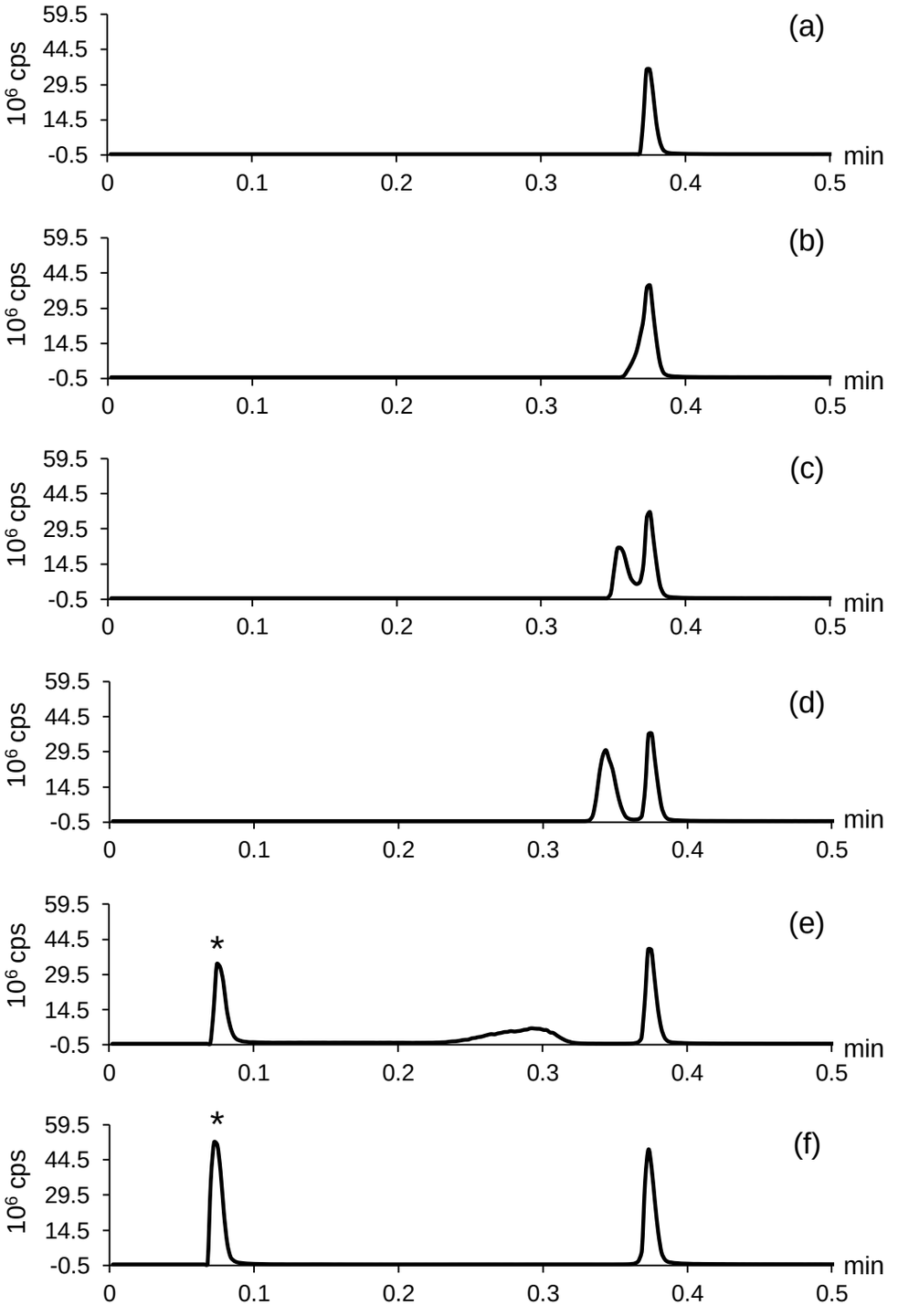

Figure 8

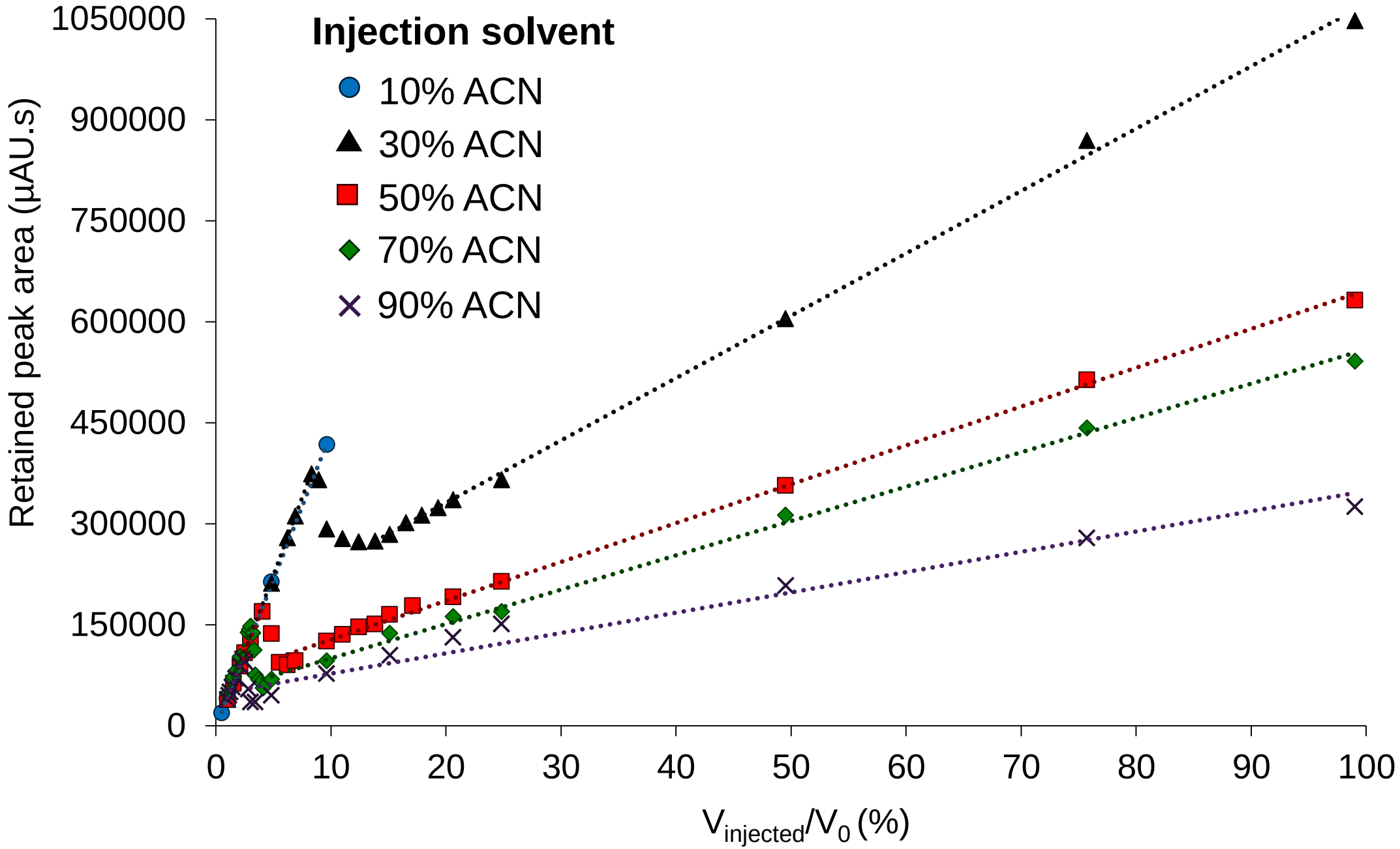
Injection solvent
10% ACN
30% ACN
50% ACN
70% ACN
90% ACN
Retained peak area (µAU.s)
1050000
900000
750000
600000
450000
300000
150000
0
0
10
20
30
40
50
60
70
80
90
100
$V_{injected}/V_0$ (%)

Figure 9

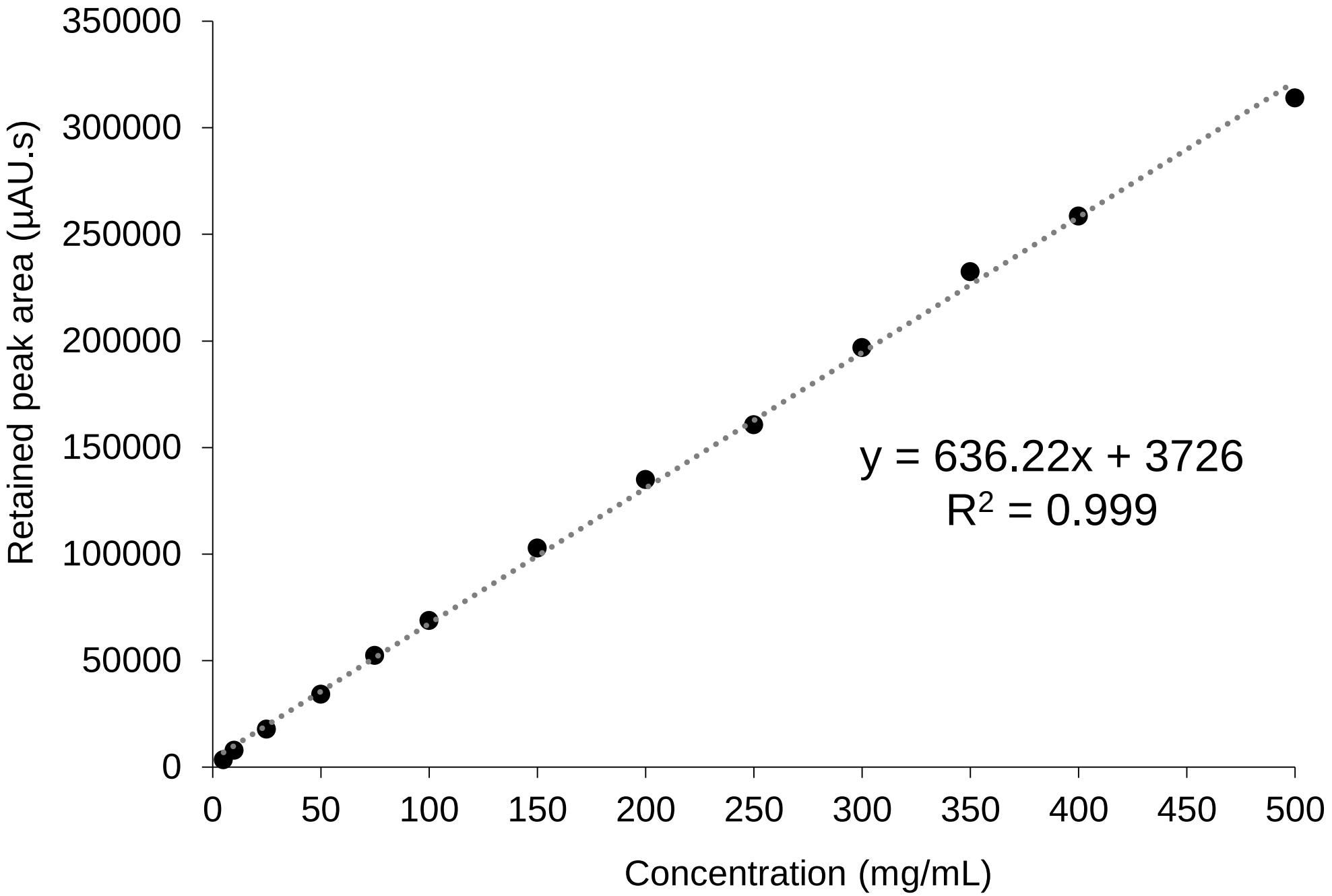
Retained peak area (µAU.s)
350000
300000
250000
200000
150000
100000
50000
0
0
50
100
150
200
250
300
350
400
450
500
Concentration (mg/mL)
y = 636.22x + 3726
R² = 0.999

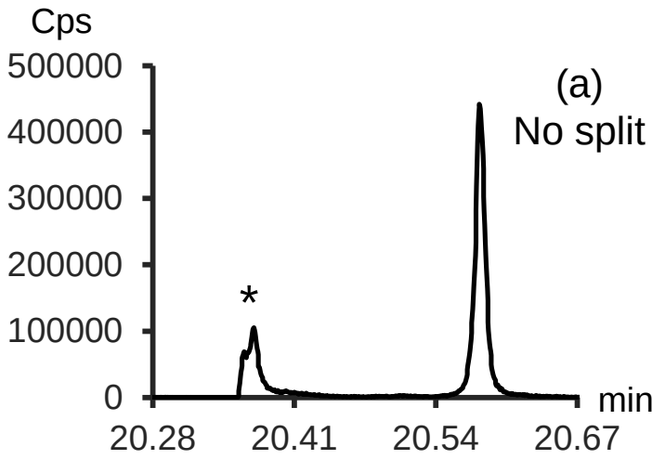
Cps
500000
400000
300000
200000
100000
0
(a)
No split
*
min
20.28
20.41
20.54
20.67

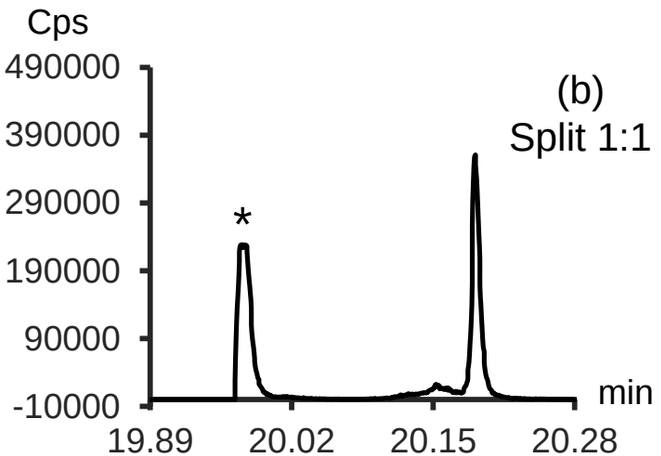
Cps
490000
390000
290000
190000
90000
-10000
(b)
Split 1:1
*
min
19.89
20.02
20.15
20.28

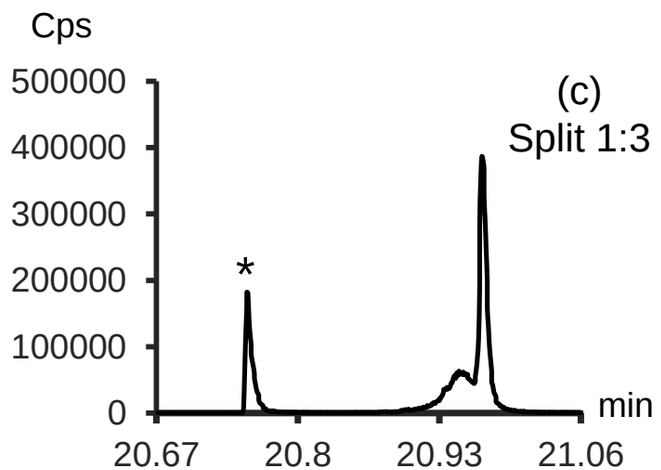
Cps
500000
400000
300000
200000
100000
0
(c)
Split 1:3
*
min
20.67
20.8
20.93
21.06

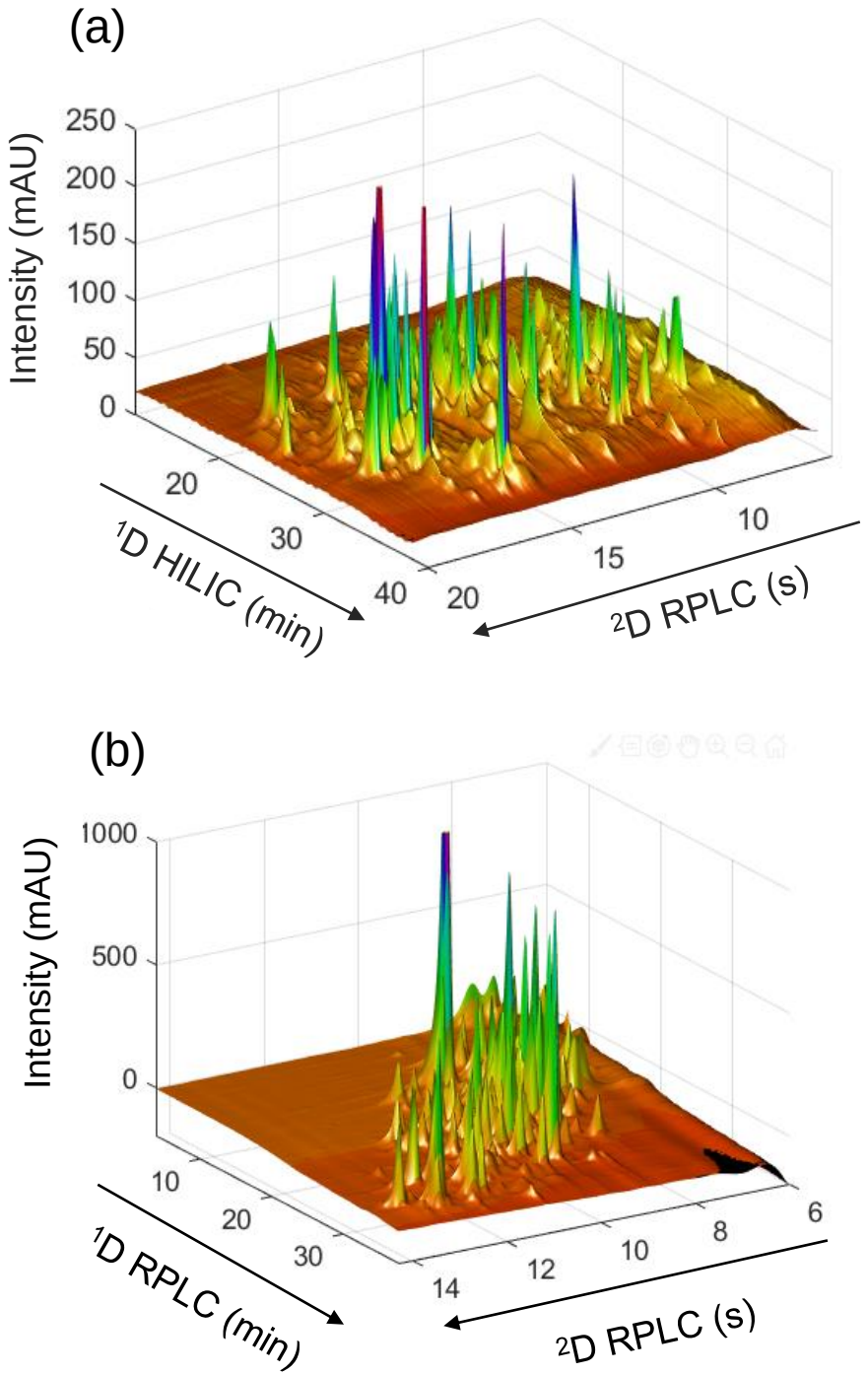
(a)
Intensity (mAU)
250
200
150
100
50
0
20
30
40
1D HILIC (min)
20
15
10
2D RPLC (s)
(b)
Intensity (mAU)
1000
500
0
10
20
30
1D RPLC (min)
14
12
10
8
6
2D RPLC (s)

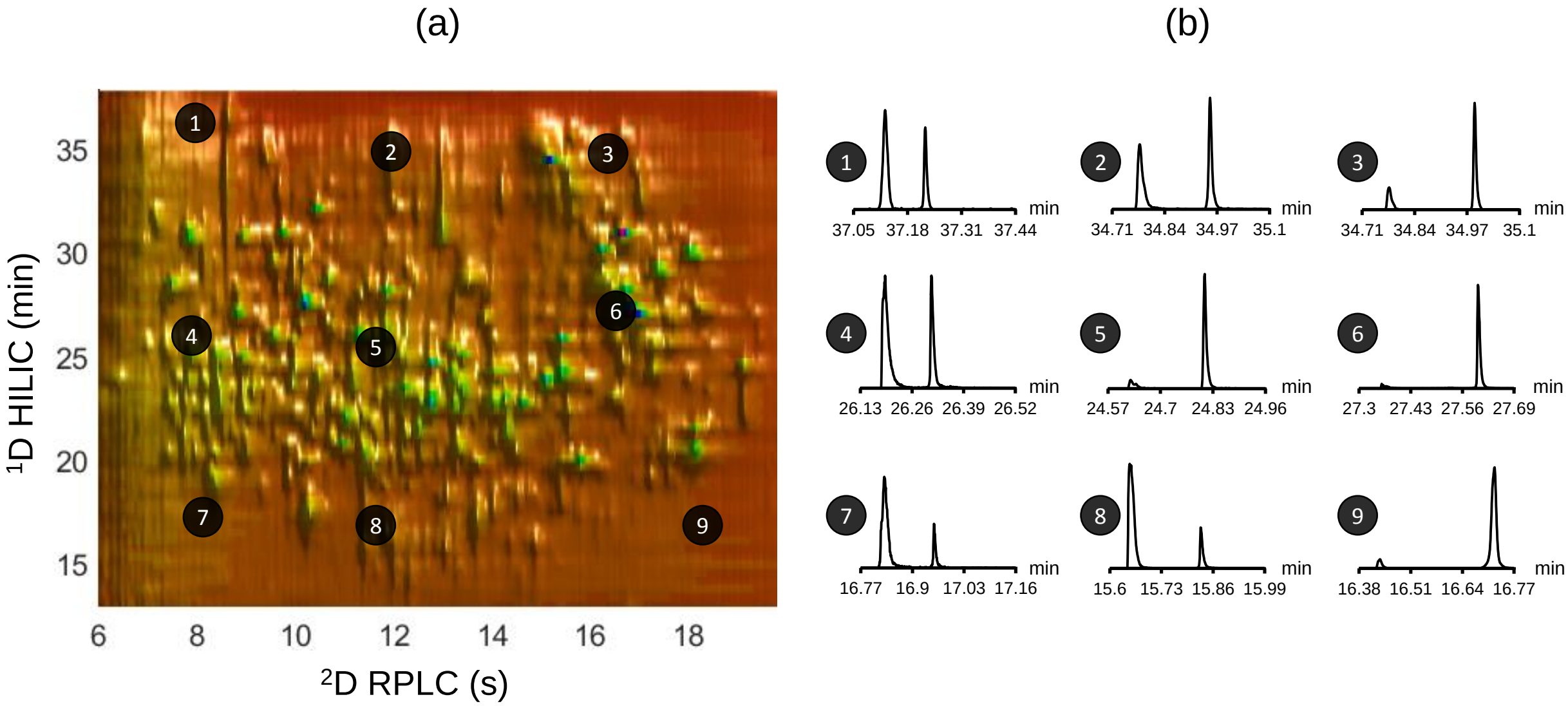
(a)
(b)
1
2
3
4
5
6
7
8
9
35
30
25
20
15
6
8
10
12
14
16
18
1D HILIC (min)
2D RPLC (s)
min
37.05 37.18 37.31 37.44
34.71 34.84 34.97 35.1
34.71 34.84 34.97 35.1
26.13 26.26 26.39 26.52
24.57 24.7 24.83 24.96
27.3 27.43 27.56 27.69
16.77 16.9 17.03 17.16
15.6 15.73 15.86 15.99
16.38 16.51 16.64 16.77

Table 1: Physical properties of the ten peptide standards used in this study.

#	Peptide name	Molecular weight (g/mol)	Isoelectric point
1	Influenza hemaglutinin (HA)	1102.15	3.5
2	FLAG® peptide	1012.97	3.9
3	WDDHH	708.68	5.2
4	Leucine enkephalin	555.62	6
5	Bombesin	1619.85	7.6
6	[arg8]-Vasopressin	1084.23	8.2
7	[ile]-Angiotensin	897.08	9.4
8	Bradykinin fragment 1-5	572.66	10.6
9	Substance P	1347.63	11.7
10	Bradykinin	1060.21	12.5

Table 2: Comparative results and specific operating conditions for the 10 studied stationary phases in HILIC.

#	**Column name** (column dimensions)	Provider (location)	Stationary phase	Flow rate (mL/min)	Gradient time[a] (min)	n_{exp}/n_{th}	Peak asymmetry	Number of peaks[b]	Elution window[c] (% B)	Derringer function
1	**Hypersil HILIC** (50 mm x 4.6 mm x 3.0 µm)	Thermo Fischer Scientific (Cheshire, UK)	Bare silica (P)	1.6	7.2	0.75	1.40	33	38	0.78
2	**Acquity BEH HILIC** (50 mm x 2.1 mm x 1.7 µm)	Waters (Milford, MA, USA)	Bare silica (H, P)	0.6	4	0.62	1.38	46	42	0.93
3	**Acquity BEH Amide** (50 mm x 2.1 mm x 1.7 µm)	Waters (Milford, MA, USA)	Amide (H, P)	0.6	4	0.38	1.74	40	39	0.69
4	**Hypersil gold HILIC** (50 mm x 2.1 mm x 1.9 µm)	Thermo Fischer Scientific (Cheshire, UK)	Bare silica (P)	0.5	4.8	0.37	2.15	26	36	0.46
5	**Nucleodur HILIC** (60 mm x 1.0 mm x 3.0 µm)	Macherey-Nagel (Duren, Germany)	Zwitterionic (P)	0.08	8.2	0.19	3.49	25	30	0.00
6	**Kinetex HILIC** (50 mm x 2.1 mm x 1.7 µm)	Phenomenex (Torrence, CA, USA)	Bare silica (SP))	0.6	2.9	0.37	1.29	38	30	0.61
7	**Nucleoshell HILIC** (100 mm x 2.0 mm x 2.7 µm)	Macherey-Nagel (Duren, Germany)	Zwitterionic (SP)	0.3	10.4	0.32	1.24	34	34	0.59
8	**Accucore HILIC** (100 mm x 2.1 mm x 2.6 µm)	Thermo fischer Scientific (Cheshire, UK)	Bare silica (SP)	0.4	8.6	0.38	1.13	40	30	0.64
9	**Luna NH_2** (150 mm x 2.0 mm x 3.0 µm)	Phenomenex (Torrence, CA, USA)	NH_2 (P)	0.3	22	0.41	1.22	29	33	0.56
10	**Cortecs HILIC** (50 mm x 2.1 mm x 1.6 µm)	Waters (Milford, MA, USA)	Bare silica (SP)	0.6	2.9	0.42	2.01	42	32	0.63

P: Totally porous particles
SP: Superficially porous particles
H: hybrid silica
n_{exp}: experimental peak capacity calculated according to Eq.5 (see Supplementary Information S3)
n_{th}: theoretical peak capacity calculated according to Eq.6 (see Supplementary Information S3)

[a] Gradient elution: 2-42% B in 20 t_0, 42% during 5 t_0, 42-2% in 1 t_0, and 2% during 10 t_0
[b] Number of peaks observed in tryptic digest sample
[c] Calculated from retention time of last and first eluted compound in tryptic digest sample

Table 3: Experimental conditions in on-line HILIC x RPLC and in on-line RPLC x RPLC (2D-separations shown in Figs. 11a and 11b respectively.

	HILIC x RPLC	RPLC x RPLC
First dimension (^{1}D)		
Injection volume	6 µL	10 µL
Injection solvent	50/50 ACN/water (v/v)	0:100 ACN/water (v/v)
Stationary phase	Acquity BEH HILIC	Ascentis express C18
Column geometry	50 mm x 2.1 mm. 1.7 µm	50 mm x 2.1 mm. 2.7 µm
Temperature	30 °C	30 °C
Mobile phase	A: ACN B: 10 mM ammonium acetate in water	A: 10 mM ammonium acetate in water B: ACN
Flow rate	0.05 mL/min	0.04 mL/min
Gradient	2-52% B in 30 min	1-34% B in 30 min
Post-column split ratio	No split for optimized method (1:1 or 1:3 for other methods)	1:2
Modulation		
Loop size	40 µL	20 µL
Sampling time	0.39 min	0.27 min
Second dimension (^{2}D)		
Stationary phase	Acquity CSH C18	Acquity CSH C18
Column geometry	(30 mm x 2.1 mm. 1.7 µm)	(30 mm x 2.1 mm. 1.7 µm)
Temperature	80 °C	80 °C
Mobile phase	A: 0.1% formic acid in water B: 0.1% formic acid in ACN	A: 0.1% formic acid in water B: 0.1% formic acid in ACN
Flow rate	2 mL/min	2 mL/min
Gradient	1-45% B in 0.26 min	1-45% B in 0.13 min
Post-column split ratio	1:2	1:2
HRMS detection		
Ionization mode	ESI^+	
Mass range	100-3200	
Scan rate	20 spectra/s	
Gas temp	300 °C	
Drying gas	11 L/min	
Nebulizer	40 psi	
Sheath gas	350 °C	
Sheath gas flow	11 L/min	
Capillary voltage	3500 V	
Nozzle voltage	300 V	
Fragmentor	150 V	
Skimmer	20 V	
Oct 1 Rf Vpp	750 V	

Table 4: Experimental results in on-line HILIC x RPLC and in on-line RPLC x RPLC for the separation of a tryptic digest of 6 proteins.

	γ	α	$^{1}w_{4\sigma}$ (min)	$^{2}w_{4\sigma}$ (s)	$\tau^{(a)}$	$n_{2D,\ effective}$
HILIC x RPLC	1	0.67	0.65	0.28	2.5	1500
RPLC x RPLC	0.56	0.70	0.49	0.30	2.7	830

(a) Effective number of fractions per peak (6σ width)